Neurexins Regulate GABA Co-release by Dopamine Neurons

Charles Ducrot[1,2,3], Gregory de Carvalho[4], Benoît Delignat-Lavaud[1,2,3], Constantin V.L. Delmas[5], Nicolas Giguère[1,2,3], Sriparna Mukherjee[1,2,3], Samuel Burke-Nanni[1,2,3], Marie-Josée Bourque[1,2,3], Martin Parent[5], Lulu Y. Chen[4,*] and Louis-Éric Trudeau[1,2,3,*]

[1]Department of Pharmacology and Physiology, Faculty of Medicine, Université de Montréal

[2]Department of Neurosciences, Faculty of Medicine, Université de Montréal

[3]Neural Signaling and Circuitry Research Group (SNC),

Montréal, QC, Canada H3C 3J7

[4]Department of Anatomy and Neurobiology,

School of Medicine, University of California,

Irvine, CA, USA 92697

CERVO Brain Research Centre, Department of Psychiatry and Neurosciences,

Faculty of Medicine, Université Laval

[*]Co-corresponding authors

Contact information:
Dr. Louis-Éric Trudeau
louis-eric.trudeau@umontreal.ca
Phone: 514-343-5692

Dr. Lulu Y. Chen
chenly@uci.edu
Phone: 949-824-3503

Summary

Midbrain dopamine (DA) neurons are key regulators of basal ganglia functions. The axonal domain of these neurons is highly complex, with a large subset of non-synaptic release sites and a smaller subset of synaptic terminals from which glutamate or GABA are released. The molecular mechanisms regulating the connectivity of DA neurons and their neurochemical identity are unknown. Here we tested the hypothesis that the trans-synaptic cell adhesion molecules neurexins (Nrxns) regulate DA neuron neurotransmission. Conditional deletion of all Nrxns in DA neurons (DAT::Nrxns KO) revealed that loss of Nrxns does not impair the basic development and ultrastructural characteristics of DA neuron terminals. However, loss of Nrxns caused an impairment of DA transmission revealed as a reduced rate of DA reuptake following activity-dependent DA release, decreased DA transporter levels, increased vesicular monoamine transporter expression and impaired amphetamine-induced locomotor activity. Strikingly, electrophysiological recording revealed an increase of GABA co-release from DA neuron axons in the striatum of the KO mice. These findings reveal that Nrxns act as key regulators of DA neuron connectivity and DA-mediated functions.

Highlights

- The study provides the first direct evidence of the role of neurexins in dopaminergic neurons
- The synaptic adhesion molecules neurexins are not required for maintaining the structure of dopamine neuron release sites.
- Neurexins regulates dopaminergic neurotransmission through regulation of dopamine reuptake, impacting amphetamine-induced locomotion
- Dopamine neurons lacking neurexins show increased GABA co-release.

Introduction

Dopamine (DA) neurons from the ventral tegmental area (VTA) and substantia nigra compacta (SNc) project densely to the ventral striatum (VS) and to the dorsal striatum (DS), respectively (Descarries et al., 1980; Matsuda et al., 2009) and are critical regulators of basal ganglia functions, motivation, and cognition (Schultz, 2007; Surmeier et al., 2014). The connectivity of the DA system is particularly intriguing due to the dual character of its axonal domain, that is predominantly non-synaptic (Descarries et al., 2008; Ducrot et al., 2021). Interestingly, the smaller synaptic subset of DA neuron terminals has the ability to co-release glutamate and GABA (Sulzer et al., 1998; Dal Bo et al., 2004; Mendez et al., 2008; Stuber et al., 2010; Tritsch et al., 2012; Tritsch et al., 2016). In contrast, the much larger contingent of non-synaptic release sites, defined as terminals not located in close apposition to a postsynaptic domain, appear to be specialized for DA release (Caille et al., 1996; Descarries et al., 1996; Descarries and Mechawar, 2000; Descarries et al., 2008; Ducrot et al., 2021). The molecular mechanisms underlying the formation and regulation of non-synaptic terminals is presently undetermined. However, a growing body of work has highlighted the functional role of trans-synaptic cell adhesion molecules such as neurexins (Nrxns) and neuroligins (NLs) in orchestrating synaptic functions and plasticity at synaptic terminals (Zhang et al 2015, Chen et al, 2017).

Nrxns are presynaptic cell adhesion molecules that were identified as α-latrotoxin receptors (Ushkaryov et al., 1992). In mammals, Nrxns are expressed in two principal forms, including longer α-neurexins isoforms and shorter ß-neurexins isoforms (Tabuchi and Sudhof, 2002). The Nrxn proteins on axon terminals interact with postsynaptic NL proteins and have been shown to regulate synapse formation and function (Ichtchenko et al., 1995; Graf et al., 2004; Ko et al., 2009). While Nrxns are the only binding partner for NLs, Nrxns have multiple postsynaptic partners and can be found as thousands of splice variants. Each Nrxn variant has differential expression, specificity and affinity for different ligands. Several key studies using a strategy of conditional Nrxns deletion in

mice demonstrated that Nrxns regulate neurotransmission through different mechanisms in a synaptic context-dependent manner (Luo 2020, 2021, Chen 2017).

Despite the functional importance of DA in the brain, a limited number of studies have until now explored the molecular mechanisms underlying the unique nature of the axonal arbor and connectivity of DA neurons (Liu et al., 2018; Robinson et al., 2019; Banerjee et al., 2020; Delignat-Lavaud et al., 2021; Ducrot et al., 2021) and none have examined the potential role of Nrxns in these neurons. Here we tested the hypothesis that Nrxns play a key role in regulating the connectivity and functions of DA neurons by deleting all Nrxns in these cells by crossing DAT-IRES-Cre mice with Nrxn123α/ß floxed mice [Nrxn123 Triple conditional KO mice (Chen et al., 2017)]. We found that the density and the ultrastructure of synapses established by DA neurons was not affected. However, electrophysiological recordings revealed that DA axon-specific optogenetically-evoked GABA-mediated synaptic currents in the KO mice were increased selectively in the ventral striatum, suggesting a negative regulatory role of Nrxns on GABA co-transmission. DA signaling was also altered after loss of Nrxns, as revealed by slower DA reuptake, decreased density of DA transporter (DAT) and increased density of vesicular monoamine transporter (VMAT2), accompanied by impaired amphetamine-induced locomotion and motor coordination compared.

Results

Dopamine neuron survival and axonal connectivity are impaired by deletion of all Nrxns.

Because Nrxns have been previously reported to influence the axonal development of neurons (Wang et al., 2019), we first examined the development of postnatal DA neurons *in vitro* and their basic connectivity. For this, we deleted Nrxn 1, 2 and 3 from DA neurons by crossing Nrxn123$^{flox/flox}$ mice with DAT-IRES-Cre mice (DAT::NrxnsKO) and prepared primary co-cultures of SNc or VTA DA neurons together with ventral striatal neurons obtained from postnatal day 0-3 pups (P0-P3), as previously described (Ducrot et al., 2021). DA neurons were identified by TH

immunocytochemistry and automated epifluorescence imaging (**Fig. 1A**). Intriguingly, the global survival of DA neurons in DAT::NrxnsKO cultures over 14 days was significantly reduced compared to WT controls (**Fig. 1B**) (main effect of genotype, Two-way ANOVA, p=0.03). However, neurite development, quantified as the number and size of TH-positive branches was not different across genotype and region **(Fig. 1C** and **3D**) (Two-way ANOVA, p=0.69).

In a second set of analyses, we also examined some of the characteristics of axon terminals established by DAT::NrxnsKO and DAT::NrxnsWT DA neurons (**Fig. 1E to 1H**). For this, fields containing axonal arbors were selected and double labeled for TH, to visualize all varicosities and the ubiquitous exocytosis Ca^{2+} sensor for Syt1. These experiments revealed that the proportion of dopaminergic varicosities containing Syt1 was not different across genotypes (**Fig. 1E, 1F, 1I**). Globally, 69.47 ± 3.60% of TH-positive dopaminergic varicosities established by SNc DA neurons in DAT::NrxnsWT cultures were positive for Syt1 (**Fig. 1E** and **1I**). For VTA neurons, this proportion was 62.03 ± 3.97%. These proportions were not significantly different for SNc and VTA DA neurons from DAT::NrxnsKO cultures (70.31 ± 3.38% and 55.60 ± 3.92%, respectively; Two-way ANOVA, p=0.93; **Fig. 1F** and **1I**). The proportion of axon terminals containing VMAT2, and thus capable of packaging DA in synaptic vesicles was also unchanged (**Fig. 1G, 1H, 1J**) (Two-way ANOVA, p=0.42). We conclude that although loss of Nrxns may decrease the resilience of DA neurons, it does not alter the intrinsic capacity of these neurons to develop an axonal domain and to establish neurotransmitter release sites.

A subset of terminals along the complex axonal arbor of DA neurons have the capacity to release glutamate or GABA (Sulzer et al., 1998; Dal Bo et al., 2004; Mendez et al., 2008; Stuber et al., 2010; Tritsch et al., 2012; Tritsch et al., 2016) We hypothesized that deletion of Nrxns could alter the formation of excitatory or inhibitory synapses by SNc and VTA DA neurons. To test this, we co-cultured DA neurons with striatal neurons and examined DAergic axon terminals in close proximity to postsynaptic organizers associated with glutamate (PSD95) and GABA (gephyrin) synapses (Craig et al., 1996; Kornau et al., 1997). We observed that loss of Nrxns reduced the

proportion of SNc, but not VTA, DA neuron terminals colocalizing with PSD95 (**Fig. 2A, 2B, 2C;** Two-way ANOVA, main effect of region, p=0.065; Sidak's multiple comparison test, SNc WT vs SNc KO DA neurons, p=0.035). Similar results were obtained with the inhibitory postsynaptic protein gephyrin, with a decrease of the proportion of SNc DA neuron terminals colocalizing with gephyrin. No change was observed for VTA DA neurons (**Fig. 2D;** Two-way ANOVA, p=0.035 Sidak's multiple comparison test, SNc WT vs SNc KO DA neurons, p=0.04). Finally, we evaluated the proportion of DA terminals expressing the glutamatergic active zone protein bassoon. In previous work, we showed that most bassoon-positive DA terminals are in close proximity to target cells, and thus most likely to be found at synapses. We found a significant decrease in the proportion of SNc DA terminals that were bassoon positive (SNc WT= 49.38 ± 6.26%; SNc KO=23.40 ± 2.55%; **Fig. 2E**). This effect was selective for SNc DA neurons as no difference was found for VTA DA neurons (**Fig. 2E**). We conclude that while loss of Nrxns did not cause a major disruption of the axonal connectivity of VTA and SNc DA neurons, these transsynaptic proteins regulate synaptic organization in a regionally-selective manner, as previously observed (Luo et al., 2020).

Nrxn123 ablation does not impair synapse ultrastructure in dopamine neurons.

We next examined synapse ultrastructure in the intact brain by transmission electron microscopy (TEM) to more directly assess a possible role of Nrxns in regulating the basic connectivity of DA neurons. We hypothesized that conditional deletion of all Nrxns would lead to an alteration of synapse integrity at the terminals of these neurons in the striatum. We focussed on terminals in the vSTR because this area contains DA neuron release sites for both glutamate and GABA in addition to those for DA (Stuber et al., 2010; Berube-Carriere et al., 2012). Overall, we found that irrespective of the genotype, most axonal varicosities contained synaptic vesicles and mitochondria (**Fig.3A** and **3B**). Furthermore, TH-positive dopaminergic terminals in the vSTR of Nrxn123 KO were not different compared to Nrxn123 WT mice in terms of their overall perimeters (P) (**Fig. 3D**; unpaired t-test, t_6=0.07; p=0.94), length (L) (**Fig. 3E**, unpaired t-test, t_6=0.72; p=0.94),

width (w) (**Fig. 3F**, unpaired t-test, t_6=0.84; *p*=0.43), or surface area (**Fig. 3G,** unpaired t-test, t_6=0.09, *p*=0.92).

In addition, the propensity of these terminals to make contact with a postsynaptic density (PSD) domain was unchanged in DAT::NrxnsKO mice. The synaptic incidence of TH-positive terminals was 6.34% (12/189 examined varicosities) for DAT::NrxnsKO mice and 4.95% (5/101 examined varicosities) for control mice, a low proportion in line with previous work (Berube-Carriere et al., 2012). The size of the PSD was also unchanged (**Fig. 3H**, unpaired t-test, t_{15}=0.61, *p*=0.54). Together these results show that loss of Nrxns123 does not impair the basic ultrastructure of DA neuron neurotransmitter release sites in the vSTR.

Deletion of Nrxns in dopamine neurons does not impair basal motor activity or motor coordination, but reduces amphetamine-induced locomotion.

The lack of extensive changes in the structural connectivity of DA neurons in mice lacking Nrnxs argues for the possibility that these proteins regulate instead some aspects of the function of these connections. We therefore next examined the behavior of conditional Nrxn123 KO mice. DA neurons and their widespread connections are key regulators of movement, motivation, and reward-dependent learning. We hypothesized that altered connectivity due to loss of Nrxns could cause impaired DA-dependent behaviors. Several studies using mouse lines with impaired DA transmission have shown deficits in basal or psychostimulant-evoked locomotion and learning on the accelerating rotarod (Zhou and Palmiter, 1995; Ogura et al., 2005; Birgner et al., 2010). In the first series of experiment, we evaluated motor coordination and learning using the accelerating rotarod task with two different protocols (**Fig. 4A**). The first protocol evaluated the rate of learning to perform this task over a total of 9 sessions during 3 days, with two sessions performed on the first day, three sessions the second day and four sessions on the third day, with a speed of rotation accelerating from 4 to 40 rpm over 10min. The measure of the latency to fall did not reveal a significant difference between the genotypes, with all groups showing a comparable increase in

performance (**Fig. 4B**, two-way ANOVA, p=0.22; WT n=8; HET n=9 and KO n=8 mice). Similar results were obtained when evaluating the progression of the performance of the mice by comparing performance on the first and last sessions, with all mice showing equivalent learning (**Fig. 4C**, paired t-test, WT (t_7 =5.15, p=0.0013); HET (t_8=4.11 p=0.034); KO (t_7=3.96 p=0.0055)). The speed of rotation at the end of each trial across all 9 trials was also unchanged (**Fig. 4D**) (two-way ANOVA, repeated measures, p=0.09). Furthermore, testing a separate cohort of mice with a more challenging version of the rotarod task (**Fig. 4A**), with speed of rotation accelerating from 4 to 40 rpm over 2 min, did not reveal that performance, calculated by the latency to fall, was significantly different in DAT::NrxnsKO and DAT::NrxnsHET compared to DAT::NrxnsWT (**Fig. 4E**, two-way ANOVA, repeated measures, p=0.07; WT n=10; HET n=14 and KO n=8 mice). In this task, performance failed to improve over the trials, revealing a limited capacity to improve performance, as shown by comparing performance in the last session compared to the first (**Fig. 4F**) (paired t-test, WT (t_9 =0.71, p=0.49); HET (t_{13}=0.89 p=0.38); KO (t_7=1.34 p=0.22)). The speed of rotation at the end of each trial across all 9 trials (**Fig. 4G**) was similar in DAT::NrxnsKO mice compared to the control mice (two-way ANOVA, repeated measures, p=0.09). These results suggest that deletion of Nrxn123 from DA neurons do not lead to motor coordination deficits.

General motor abilities were next evaluated using the pole test and the open field test. In the pole test (**Fig. S1A**), no difference was observed between genotypes for the time required for the mice to orient downward (**Fig. S1B)** (one-way ANOVA, p=0.4) and for the time required to climb down the pole (**Fig. S1C)** (one-way ANOVA, p=0.07; WT n=10; HET n=11 and KO n=7 mice). Basal locomotion in the open field over a 60-min period was also not different between genotypes (**Fig. 4H**; WT n=10; HET n=11 and KO n=10 mice). We next challenged the dopaminergic system of these mice using the psychostimulants cocaine and amphetamine. Although locomotion induced by cocaine (5mg/kg) was comparable between genotypes (**Fig. 4I**, Two-way ANOVA, p=0.67; WT n=10; HET n=11 and KO n=8 mice), locomotion induced in

response to amphetamine (Di Chiara and Imperato, 1988) was strongly reduced in DAT::NrxnsKO mice compared to DAT::NrxnsHET and DAT::NrxnsWT mice (**Fig. 4J**, two-way ANOVA, p=0.0001). The maximal effect was observed between 30 to 40 min post-injection (**Fig. 4J**; Two-way ANOVA, Tukey's multiple comparison test, DAT::NrxnsKO vs WT. t=50min: p=0.03; t=55min: p=0.01; t=60min: p=0.02; WT n=7; HET n=7 and TKO n=8 mice). These results suggest that loss of Nrxns in DA neurons leads to altered DA neurotransmission and DA-dependent behaviors.

Because altered DA neurotransmission is often associated with altered motivational states, we next examined the performance of the mice in a well-established sucrose preference task. On the initial two conditioning days (CD1 and CD2), mice of all genotypes equally licked at both bottles **(Fig. 4K, 4L)**. Similarly, during the next 3 testing days (TD1, 2 and 3), when mice were given the choice between water and sucrose, DAT::NrxnsKO, HET and WT mice showed a similar marked preference for the sucrose bottle (**Fig. 4L).** These findings suggest that the response of mice to natural rewards was unaltered by loss of Nrxns in DA neurons.

Fast Scan Cyclic Voltammetry reveals normal DA release but slower reuptake and enhanced paired-pulse depression after conditional deletion of all Nrxns in DA neurons.

The impaired response to amphetamine suggests a perturbation of extracellular DA dynamics or DA action on target cells. To examine this possibility, we first employed fast scan cyclic voltammetry (FSCV) to measure electrically-evoked DA overflow in acute brain slices of the ventral and dorsal striatum (vSTR and dSTR). In the dSTR, we found no difference in peak DA overflow between the DAT::NrxnsWT and DAT::NrxnsKO mice (1.33 ± 0.05µM and 1.35 ± 0.07µM, respectively), but surprisingly, in the DAT::NrxnsHET mice, peak DA release was significantly lower (1.05 ± 0.05µM; One-way ANOVA, p=0.001, Dunnett's comparison test, WT vs HET, p=0.002 and HET vs KO, p=0.006) compared to the WT and KO mice (**Fig. 5A** and **5B**). An examination of the kinetics of DA overflow, often used to identify changes in DA release

efficiency and reuptake (Yorgason et al., 2011), suggested that DA reuptake was significantly slower in the dSTR of DAT::NrxnsKO and DAT::NrxnsHET compared to the DAT::NrxnsWT mice (One-way ANOVA, main effect of genotype, p=0.0037) as illustrated by higher Tau values (**Fig. 5A** and **5C**; KO= 0.45 ± 0.03; HET= 0.47 ± 0.02; WT= 0.36 ± 0.02, WT vs KO p=0.034; WT vs HET p=0.041). A similar difference was also detected in the vSTR (**Fig. 5E** and **5G;** One-way ANOVA, main effect of genotype, p=0.0037; KO= 0.45 ± 0.03; HET= 0.47 ± 0.02; WT= 0.36 ± 0.02, WT vs KO p=0.034; WT vs HET p=0.041).

Quantification of the rise-time of evoked DA overflow in the dSTR revealed a slower rise time in DAT::NrxnsHET mice compared to DAT::NrxnsWT mice (**Fig. S2A;** 0.25 ± 0.01s compared to 0.22 ± 0.01s, respectively, one-way ANOVA, Holm-Šidák's multiple comparison test, p=0.044). No differences were found in the vSTR (**Fig. S2B)**.

Short-term plasticity of electrically evoked DA release in striatal sections was examined using a paired-pulse stimulation paradigm (inter-pulse interval (IPI) of 100ms). DA overflow in acute brain slices typically shows a large paired-pulse depression, more extensively so in the dSTR compared to the vSTR (Zhang and Sulzer, 2004; Sanchez et al., 2014; Condon et al., 2019). We found that the level of paired-pulse depression was similar in DAT::NrxnsKO mice compared to the WT group in the dSTR (**Fig. 5D)** (Two-way ANOVA, Tukey's multiple comparison, p=0.022). However, in the vSTR, paired-pulse depression was significantly enhanced in DAT::NrxnsKO mice compared to WT (**Fig. 5H**; Two-way ANOVA, Tukey's multiple comparison, p=0.022). Plasticity of DA overflow was also examined by measuring the inhibition of DA overflow induced by the $GABA_B$ agonist baclofen (10μM) (Lopes et al., 2019). This was particularly interesting to examine in light of the results of a recent study demonstrated a role for Nrxns in the regulation of the expression and location of presynaptic $GABA_B$ receptors (Luo et al., 2021). Baclofen induced a robust decrease of evoked DA overflow, however, this was not different across genotypes (**Fig. S1C**; Two-way ANOVA, p=0.93).

Together these observations suggest that Nrxns, while not required for DA release, play a role in regulating DA neurotransmission, including through regulation of DA reuptake and short-term plasticity in the vSTR.

GABA release by dopamine neurons is increased in the ventral striatum of DAT::NrxnsKO mice.

Whole-cell patch-clamp electrophysiological recordings in medium spiny neurons of the vSTR and dSTR in DAT::NrxnsWT, HET and KO littermates were next performed to examine the role of Nrxns in synaptic GABA and glutamate release by DA neurons. ChR2-EYFP was selectively expressed in DA neuron axons using a conditional AAV construct (**Fig. 6A**). Most DA neurons in the VTA and SNc were infected by the virus as revealed by the presence of strong EYFP signal (**Fig. 6B**). We first pharmacologically isolated GABA-mediated inhibitory synaptic currents evoked by optical stimulation of DA neurons axons (oIPSC) and found a significant increase in the amplitude of oIPSCs in the DAT::NrxnsKO slices (**Fig. 6C**), with no change in electrically evoked GABA synaptic currents (eIPSC; **Fig. S3A**). Interestingly, the frequency of spontaneous IPSCs (sIPSCs) was also significantly increased in the KO group (**Fig. 6D**). As expected, oIPSCs were blocked by picrotoxin (50 µM), confirming their GABAergic nature (**Fig. S4A**). Disruption of VMAT2 function using reserpine (1µM) also blocked oIPSCs, in line with previous work showing that GABA release by DA neurons paradoxically requires VMAT2 (Tritsch et al., 2012; Tritsch et al., 2014) (**Fig. S4C**).

Closer analysis of the kinetics of GABA-mediated oIPSCs in the ventral striatum revealed a significant slowing of oIPSC decay time (**Fig. 6E, S5A-D**) and decay time constant (**Fig. S5)** in both DAT::NrxnsKO and DAT::NrxnsHET mice. These findings thus reveal that neurexin deletion in ventral striatal DAergic terminals prolongs GABAergic activity in MSNs.

As our manipulation affected the entire mesolimbic pathway, we also performed parallel optical stimulation and recordings in the dorsal striatum. We observed no statistically significant changes in oIPSC amplitude in DAT::NrxnsKO mice in the dorsal striatum (**Fig. 6F**). Spontaneous and electrically-evoked GABA IPSCs were also unaltered (**Fig. 6G**, **Fig. S3C and S3D**), as was oIPSC decay time (**Fig. 6H** and **S6E-H**).

Together these results suggest that Nrxns act as regulators of GABA co-transmission by DA neurons in a regionally-selective manner. Further work will be required to identify the origin of this selectivity.

Optically evoked excitatory transmission is unaltered in the striatum of DAT::NrxnsKO mice.

We also examined glutamate release by DA neurons in the ventral and dorsal striatum and did not detect differences in optically-evoked glutamate-mediated EPSCs (oEPSCs) in the two regions (**Fig. 7A, 7B**). The frequency and amplitude of spontaneous EPSCs (sEPSCs) was also unchanged (**Fig. 7C, 7D**). The paired-pulse ratio and input-output relationship of electrically-evoked IPSCs were similarly unchanged (**Fig. S5**). These results suggest that Nrxns do not have a major role in regulating glutamate release from DA neurons. However, surprisingly, we detected a significant increase of the amplitude of EPSCs evoked by local electrical stimulation in the ventral (**Fig. S3B**) but not the dorsal (**Fig. S3D**) striatum. This observed increase in eEPSC amplitude opens the possibility that deletion of Nrxns impacts the development of DAergic projections to non-striatal regions that project to ventral striatum.

Altered GABA uptake and VMAT2 suggest a possible mechanism underlying increased GABA release in Nrxns KO mice.

The region-specific increase of GABA release from DA axons in DAT::NrxnsKO mice, identified in our optogenetic experiments, could result from different mechanisms. One possibility

is that loss of Nrxns induced differential adaptations in the expression of some of the postsynaptic partners of Nrxns, including NLs. However, using qPCR, we did not detect major changes in expression of these genes in microdissected vSTR or dSTR, except for a small decrease in collybistin and LRRTM3 mRNA in DAT::NrxnsKO mice (unpaired t-test, p=0.021 and p=0.014, respectively) (**Fig. S7A** and **S7B**).

While DA neurons have the capacity to co-release GABA, it is well established that they do not synthetize it using glutamic acid decarboxylase and do not express the vesicular GABA transporter (Tritsch et al., 2012; Tritsch et al., 2014). Instead, they have been shown to use plasma membrane transporters to uptake GABA from the extracellular medium and VMAT2 to package it into synaptic vesicles (Tritsch et al., 2012; Tritsch et al., 2014). We therefore used a GABA uptake assay using primary DA neurons and quantified VMAT2 levels in the striatum.

GABA uptake was estimated using cultures prepared from DA neurons co-cultured with vSTR or dSTR neurons. Neurons were incubated with GABA (100µM) for 2h, rapidly washed and fixed before quantification of GABA immunoreactivity in these neurons, evaluating the proportion of TH signal in DA axons covered by GABA immunoreactivity in comparison to a control group treated with H_2O (**Fig. 8A**). This treatment induced a robust increase in GABA immunoreactivity in DA neuron axons (**Fig. 8B** to **8D**). Interestingly, SNc DA neurons globally showed a larger GABA uptake compared to VTA DA neurons (**Fig. 8E**; Main effect of region; two-way ANOVA, p<0.001, F(1, 76=53.35). Furthermore, we observed a global increase of GABA uptake in DAT::NrxnsKO DA neurons compared to DAT::NrxnsWT DA neurons (two-way ANOVA, main effect of genotype, p=0.014).

We next examined the level of VMAT2 in DA neuron axons in the striatum of DAT::NrxnsKO mice compared to controls, as well as TH and DAT. A first global quantification of striatal tissue levels by Western Blot (**Fig. S8A and S8E**), revealed a lack of overall change in the levels of TH and VMAT2 in DAT::NrxnsKO mice, in both vSTR and dSTR (**Fig. S8B, S8C, S8F and S8G**). However, DAT levels were significantly reduced in the vSTR (**Fig. S8A** and **S7D**;

unpaired t-test, t_{10}=2.79; *p*=0.019). We also observed a strong tendency for a similar decrease in DAT in the dSTR (**Fig. S8E** and **S8H;** unpaired t-test, t_{10}=1.93; *p*=0.081).

To gain more region-specific insight in the levels of these proteins, we measured the intensity and surface area for these markers in a series of 3 striatal sections ranging from bregma +0.74 to bregma -0.82 mm, with a total of 7 different regions in each hemisphere (**Fig. 9A**). In this experiment, all sub-regions compared and analyzed separately. First, TH signal intensity (**Fig. 9B, 9C and 9F**) and TH surface area (**Fig. 9G**) were unchanged in both dSTR and vSTR. For VMAT2 immunoreactivity, although intensity was unchanged (**Fig. 9B, 9C** and **9H**), surface area was increased in both the vSTR and in the rostral part of the dSTR (**Fig. 9I**) (vSTR= 169.3 ± 28.42% of control, unpaired t-test, Welch's correction, *p*=0.045; dSTR1= 142.4 ± 11.14%; dSTR2= 120.8 ± 12.73%; dSTR3= 143.3 ± 32.98% of control; unpaired t-test, Welch's correction, *p*=0.045). DAT immunostaining showed an opposite change in DAT::NrxnsKO mice, with a decrease of signal intensity in the vSTR (**Fig. 9D** and **9J**) (vSTR=74.07 ± 20.98% of control; unpaired t-test, *p*=0.039) and in the rostral and caudal parts of the dSTR (**Fig. 9D, 9E** and **9J**; dSTR1= 80.50 ± 17.77%; dSTR2= 93.17 ± 21.96%; dSTR3= 72.80 ± 17.08% of control). The DAT surface area was also significantly decreased in the vSTR and in the caudal part of the dSTR (**Fig. 9K**; vSTR=58.92 ± 10.72% of control; Unpaired t-test, *p*=0.033; dSTR1= 60.80 ± 3.87%; dSTR2= 95.98 ± 3.38%; dSTR3= 62.78 ± 6.71% of control; unpaired t-test, Welch's correction *p*=0.030).

Together, our observation of increased GABA uptake and increased VMAT2 in the vSTR could represent an explanation for the observed increase in GABA release by DA neuron axons in this part of the striatum.

Discussion

Since the initial discovery of Nrxns (Ushkaryov et al., 1992), a large number of studies have explored the roles of these proteins in synapse formation, function, maintenance and plasticity. Most of these studies have been conducted on glutamatergic or GABAergic neurons, with no

evaluation of their role in modulatory neurons like DA, serotonin, norepinephrine of acetylcholine neurons, whose connectivity is strikingly different and drastically less synaptic (Ducrot et al., 2021). We hypothesized that new insights could be gained by studying the role of such trans-synaptic proteins in modulatory neurons. In the present study, we therefore took advantage of a recently introduced triple conditional Nrxn mouse line (Chen et al., 2017) to selectively delete Nrxns in DA neurons and examine the impact of this gene inactivation using a combination of primary neuronal cultures, electron microscopy, behavioral assessments, patch-clamp recording of GABA and glutamate release, fast scan cyclic voltammetry and immunohistochemistry. We found that while loss of Nrxns does not markedly impair the basic development and axonal ultrastructure of DA neuron terminals *in vitro* and *in vivo*, this leads to region-specific changes in their axonal connectivity. We also found that loss of Nrxns is associated with impaired DA neurotransmission in the brain of adult mice, as revealed by a reduced rate of DA reuptake after electrically-evoked DA release and with impaired amphetamine-induced locomotion. Patch-clamp recordings of GABA and glutamate release by DA neuron axons also revealed an unexpected increase of GABA co-release. Together these findings suggest that although Nrxns are not critical for many aspects of the basic axonal development and synapse formation of DA neurons, they act as key regulators of GABA and DA signalling in these neurons.

Nrxns are not required for the basic morphological development but regulate the connectivity of DA neurons

Nrxns have been previously suggested to contribute to the development of synapses (Missler et al., 2003; Li et al., 2007; Etherton et al., 2009; Aoto et al., 2015; Chen et al., 2017). In a first series of experiments, we examined whether loss of Nrxns impairs the morphological development of DA neurons. For this, we established co-cultures of VTA and SNc DA neurons with vSTR and dSTR neurons and astrocytes. Our results did not identify major change in global axonal development of these neurons. However, we found that the proportion of bassoon-positive terminals established by

SNc DA neurons was reduced after loss of Nrxns and that the proportion of these terminals contacting PSD95 postsynaptic domains was also reduced suggests that these proteins play a role in regulating the active zone and fine connectivity of DAergic terminals. This finding is in line with recent results suggesting a possible role of Nrxns in the organizational features of the active zone (Luo et al., 2020). How Nrxn-123 organize active zone assembly is presently unknown, but previous studies suggest that Nrxns can interact indirectly with active zone proteins through calcium/calmodulin-dependent serine protein kinase 3 and membrane-associated guanylate kinase 2 (CASK) protein (Hata et al., 1996). Further experiments will be needed to evaluate this possibility more directly using transmission electron microscopy or other types of high-resolution microscopy approaches. Compatible with these *in vitro* results, in adult DAT::Nrxn triple KO mice, we also found no evidence of any gross morphological disruptions of the mesotelencephalic DA system (results not shown), although further quantitative work will be required to validate this conclusion.

Experiments performed *in vitro* allowed us to more closely examine the propensity of DA terminals to interact with GABA and glutamate postsynaptic domains. This was particularly interesting because of the well-known capacity of these neurons to co-release glutamate and GABA in a subset of their synaptic terminals (Sulzer et al., 1998; Dal Bo et al., 2008; Descarries et al., 2008; Stuber et al., 2010; Tritsch et al., 2012), and because we hypothesized that Nrxns might regulate the establishment of excitatory and inhibitory synapses by DA neurons. Quantification of the proportion of TH-positive terminals overlapping with the glutamatergic postsynaptic marker PSD95 revealed a decrease in the proportion of SNc DA neuron terminals contacting a PSD95 or gephyrin postsynaptic domain in cultures prepared from DAT::NrxnsKO mice. However, results obtained with transmission electron microscopy in striatal sections did not reveal any differences in the ultrastructure of DA terminals in these mice in comparison to wild type controls. These data suggest that although Nrnxs are not required for the basic structure of DA neuron terminals, they can regulate DA neuron connectivity in a region-specific manner. This finding is in agreement with previous reports obtained with single, double or triple deletion of Nrxn in glutamatergic or

GABAergic neurons (Missler et al., 2003). The first *in vivo* study on the conditional triple Nrxn deletion, published by Chen and colleagues in 2017, reported the same negative effect on synapse formation by somatostatin-positive interneurons in the cerebral cortex. However, removal of Nrxns resulted in a significant decrease in the number of parvalbumin-positive synapses in the cortex and of excitatory synapses formed by the climbing fibers innervating purkinje neurons in the cerebellum. Another recent study using the triple Nrxn mice also reported a lack of impact of Nrxn deletion on synapse formation at the calyx of Held (Luo et al., 2020). Taken together with our results, we similarly conclude that Nrxns play a synapse-specific regulatory role in synapse formation and maintenance and do not act as direct drivers of synapse formation.

Dopamine transporter function is altered in DAT::NrxnsKO mice

To obtain direct functional insight in the roles of Nrxns in DAergic neurotransmission, we performed FSCV recordings in the vSTR and dSTR. Our data revealed that peak electrically-evoked DA overflow was not reduced in the absence of Nrxns, suggesting that Nrxn123 do not play an obligatory role in the DA release mechanism and the initial formation and function of DA neuron varicosities, in line with our *in vitro* results. The reduction in peak DA overflow in DAT::NrxnsHET mice is puzzling and remains presently unexplained. One possibility is that deletion of a single Nrxn123 allele was insufficient to prevent the occurrence of possible compensatory mechanisms induced in full knockouts. Although peak DA release was not impaired in the absence of Nrxns, we found a systematic impairment in DA reuptake in both DAT::NrxnsKO and DAT::NrxnsHET mice compared to DAT::NrxnsWT mice. This finding of impaired DAT function is particularly intriguing in the context of our observation that DAT::NrxnsKO mice show a robust impairment in amphetamine-induced locomotion. Amphetamine is well known to increase extracellular DA levels by impairing vesicular storage of DA and inducing reverse transport through the DAT. It is thus possible that Nrxns regulate the stability and function of the DAT in

DA neuron axon terminals and that in the absence of Nrxns, DAT function and positioning in terminals is impaired.

Possible regulatory role of Nrxns in GABA release by dopamine neurons

One of the most intriguing observations in the present study is the increase of evoked GABA release from VTA DA neuron terminals in the vSTR but not from SNc DA neurons projecting to the dSTR. This result suggests a region-specific role of Nrxns in regulating GABA co-release by DA neurons. The origin of this selectivity is presently unclear but could result for example from differential presynaptic Nrxn isoform expression in both regions. For example, if NRXN2 is more prevalent than NRXN1 and NRXN3 in dopaminergic terminals in the ventral striatum, this would result in a different role for Nrxns within that region. It is now well established that the functional consequences of Nrxn deletion differ between neuronal subtypes and species. Multiple studies over the past decade reported similar conclusions, where different Nrxn isoforms were proposed to regulate various aspects of synapse organization and function (Ullrich et al., 1995). One recent interesting study illustrates this difference, where a double deletion of both Nrxn-3αß had a differential effect at glutamate and GABA synapses, with a reduction of postsynaptic AMPA receptors at excitatory synapses in hippocampal neurons, and a decrease in presynaptic release probability at olfactory bulb inhibitory synapses (Aoto et al., 2015). Similarly, in the present study, our work suggests that Nrxns preferentially regulate the function of GABA synapses. The role of these proteins in regulating glutamate synapses established by DA neuron axons is less clear. Although we detected a decrease in the propensity of DA neuron axonal varicosities to contact PSD95 postsynaptic domains, we did not detect a decrease in optically-evoked glutamate-mediated EPSCs in striatal neurons in slices prepared from DAT::NrxnsKO mice. This dichotomy suggests that although structural changes may have happened at these glutamatergic terminals, this did not translate into functional changes. These findings highlight the complexity and the diversity of the role of Nrxns at synapses, in line with much recent work (Chen et al., 2017; Luo et al., 2020).

A possible hypothesis to explain our observations is that one or more Nrxns act as a repressor of GABA co-transmission and thus regulate the excitatory/inhibitory neurotransmission balance of the axonal domain of DA neurons. Indeed, previous work has shown that Nrxns physically and functionally interact with $GABA_A$ receptors and that overexpression of Nrxns decreases inhibitory but not excitatory synaptic strength (Zhang et al., 2010). These results are consistent with our observations showing that after removal of all Nrxns, GABAergic synaptic events evoked by stimulation of DA neuron terminals is increased. Further work, including rescue experiments would be needed to test this hypothesis directly and determine which Nrxn is involved in this mechanism.

It would also be interesting to complement our work by recording separately from striatal MSNs of the direct and indirect basal ganglia pathway (Gerfen and Surmeier, 2011), as it is possible that some of the heterogeneity in our results on GABA and glutamate synaptic events derive from differences in the roles of Nrxns in these two pathways. Previous work has shown that DA regulates tonic inhibition in striatal MSNs and this regulation differs between D1 and D2 MSNs (Janssen et al., 2009). Given our results of GABA release from DA terminals, investigating tonic inhibition of D1 and D2 MSNs within the context of Nrxn deletion would be of interest for future work.

Mechanistically, the increase in GABA IPSCs we detected in DAT::NrxnsKO mice may have resulted from either pre- or postsynaptic changes. In line with presynaptic changes, we detected an increase in GABA uptake by cultured DA neurons as well as in increase in VMAT2 levels, detected in striatal sections. Together these two mechanisms could lead to increased GABA uptake by DA neuron terminals and to increased GABA vesicular packaging through a VMAT2-dependent process. The prolongation of optically-evoked IPSCs that we also detected in slices prepared from DAT::NrxnsKO mice could in principle reflect either a prolongation of the kinetics of GABA release or a prolongation of $GABA_A$ receptor opening. Further experiments will be requited to distinguish between these possibilities.

Alterations in DA neuron connectivity secondary to loss of Nrxns may also possibly regulate the intrinsic vulnerability of DA neurons, as suggested by our observation of reduced survival of DA neurons in primary cultures established from DAT::NrxnsKO mice. Because we did not observe a decrease in TH signal in the striatum of these mice, we did not perform stereological counting of DA neurons in these mice or investigate their vulnerability in Parkinson's disease models, but this may be of interest in future experiments.

Together, our findings shed new light on the role of these cell-adhesion molecules in DA neuron connectivity. We conclude that Nrxns are dispensable for the initial establishment of axon terminals and synapses by DA neurons but play a role in regulating both DAT function and GABA release by DA neurons. Only a small subset of axon terminals established by DA neurons adopt a synaptic configuration. We conclude that the formation of such synaptic contacts must be regulated by other transsynaptic proteins, including potential candidates such as PTP-sigma. As we observed a robust decrease in bassoon positive terminals established by DA neurons in the absence of Nrxns, it remains possible that these trans-synaptic proteins play a role in regulating active zone assembly in a subset of terminals established by DA neurons. Further experiments will be needed to determine if this assembly is subject to control by presynaptic signals or if it is controlled more indirectly by trans-synaptic signaling via postsynaptic signals.

STAR methods

Animals

All procedures involving animals and their care were conducted in accordance with the Guide to care and use of Experimental Animals of the Canadian Council on Animal Care. The experimental protocols were approved by the animal ethics committees of the Université de Montréal (CDEA). Housing was at a constant temperature (21°C) and humidity (60%), under a fixed 12h light/dark cycle with food and water available ad libitum.

Generation of triple Neurexins cKO mice in DA neurons

All experiments were performed using mice generated by crossing DAT-IRES-Cre transgenic mice (Jackson Labs, B6.SJL-Slc6a3tm1.1 (Cre)Bkmn/J, strain 006660) with Nrxn123loxP mice [for details see (Chen et al., 2017)]. Briefly, conditional knock-out (cKO) mice were produced as a result of CRE recombinase driving a selective excision of Nrxn-1, Nrxn-2 and Nrxn-3 genes in DA neurons and giving three different genotypes: Nrxn123 KO, Nrxn123 HET and Nrxn123 WT mice. The Nrxn123flox/flox mice were on a mixed Cd1/BL6 genetic background. The DAT-IRES-Cre mice was on a C57BL/6J genetic background. Except for culture experiments, only males were used.

Genotyping

Mice were genotyped with a KAPA2G Fast HotStart DNA Polymerase kit (Kapa Biosystem). The following primers were used: DAT-IRES-Cre: Common 5' TGGCTGTTGTGTAAAGTGG3', wild-type reverse 5'GGACAGGGACATGGTTGACT 3' and knock-out reverse 5'-CCAAAAGACGGCAATATGGT-3', Nrxn-1 5'-GTAGCCTGTTTACTGCAGTTCATT-3' and 5'-CAAGCACAGGATGTAATGGCCTT-3', Nrxn-2 5'-CAGGGTAGGGTGTGGAATGAG-3' and 5'-GTTGAGCCTCACATCCCATTT-3', Nxn3 5'-CCACACTTACTTCTGTGGATTGC-3' and 5'-CGTGGGGTATTTACGGATGAG-3'.

Primary neuronal co-cultures

For all experiments, postnatal day 0-3 (P0-P3) mice were cryoanesthetized, decapited and used for co-cultures according to a previously described protocol (Fasano et al., 2008). Primary VTA or SNc DA neurons were obtained from Nrxn123 KO or Nrxn123 WT pups and co-cultured with ventral striatum and dorsal striatum neurons, respectively from Nrxn123 KO or Nrxn123 WT pups. Neurons were seeded on a monolayer of cortical astrocytes grown on collagen/poly-L-lysine-coated

glass coverslips. All cultures were incubated at 37°C in 5% CO_2 and maintained in 2/3 of Neurobasal medium, enriched with 1% penicillin/streptomycin, 1% Glutamax, 2% B-27 supplement and 5% fetal bovine serum (Invitrogen) plus 1/3 of minimum essential medium enriched with 1% penicillin/streptomycin, 1% Glutamax, 20mM glucose, 1mM sodium pyruvate and 100 µl of MITO+ serum extender. All primary neuronal co-cultures were used at 14DIV.

Immunocytochemistry on cell cultures

Cultures were fixed at 14-DIV with 4% paraformaldehyde (PFA; in PBS, pH-7.4), permeabilized with 0,1% triton X-100 during 20-min, and nonspecific binding sites were blocked with 10% bovine serum albumin during 10-min. Primary antibodies were: mouse anti-tyrosine hydroxylase (TH) (1:2000, Sigma), rabbit anti-TH (1:2000, Chemicon), rabbit anti-synaptotagmin 1 (Syt1) (1:1000, Synaptic Systems) and rabbit anti-vesicular monoamine transporter 2 (VMAT2) (1:1000, gift of Dr. Gary Miller, Colombia University). To improve the immunoreactivity of the synaptic markers PSD95, gephyrin and bassoon, a set of cultures were fixed with 4% PFA together with 4% sucrose. For these experiments, the primary antibodies were mouse anti-PSD95 (1:1000 Pierce antibody), mouse anti-gephyrin (1:1000, Synaptic Systems) and guinea pig anti-bassoon (1:1000, Synaptic Systems). These were subsequently detected using Alexa Fluor-488-conjugated, Alexa Fluor-546-conjugated, Alexa Fluor-568-conjugated or Alexa Fluor-647-conjugated secondary antibodies (1:500, Invitrogen).

Transmission Electron Microscopy (TEM)

Following i.p. injection of ketamine (100 mg/Kg) and xylazine (10 mg/Kg), mice were transcardially perfused with 50 ml of ice-cold sodium phosphate buffer saline (PBS; 0.1M; pH 7.4) followed by 150 mL of a mix composed of 4% paraformaldehyde and 0.1% glutaraldehyde diluted in PBS. Dissected brains were extracted and post-fixed overnight in 4% PFA at 4˚C. Mouse brains were cut with a vibratome (model VT1200 S; Leica, Germany) into 50 µm-thick transverse sections.

For TH immunostaining, 50 µm-thick sections taken through the striatum (1.18 mm and 1.34 mm from bregma, according to the mouse brain atlas of Franklin & Paxinos 1st edition) were rinsed with PBS and pre-incubated for 1h in a solution containing 2% normal goat serum and 0.5% gelatin diluted in PBS. Sections were then incubated overnight with a rabbit primary TH antibody (Millipore, catalogue no. AB152, 1/1000). Sections were rinsed and incubated during 2h with a goat anti-rabbit secondary antibody (1/500) and directly coupled to a peroxidase (Jackson, catalogue no. 111-035-003). The peroxidase activity was revealed by incubating sections for 5 min in a 0.025 % solution of 3,3' diaminobenzidine tetrahydrochloride (DAB; Sigma-Aldrich, catalogue no. D5637) diluted in Tris-saline buffer (TBS; 50 mM; pH 7.4), to which 0.005% of H_2O_2 was added. The reaction was stopped by several washes in TBS followed by phosphate buffer (PB; 50 mM; pH 7.4). At room temperature, sections were washed 3 times in ddH_2O and incubated for 1h in a solution composed of 1.5% potassium ferrocyanide and 2% osmium tetroxide (EMS) diluted in ddH_2O. After 3 rinses in ddH_2O, sections were incubated for 20 min in a filtered solution of 1% thiocarbohydrazide (Ted Pella) diluted in ddH_2O. Sections were then rinsed 3 times and incubated in 2% osmium tetroxide. After rinses in ddH_2O, sections were dehydrated in graded ethanol and propylene oxide and flat-embedded in Durcupan (catalogue no.44611-14; Fluka, Buchs, Switzerland) for 72h at 60˚C. Trapezoidal blocs of tissue from the ventral striatum were cut from the resin flat-embedded TH-immunostained sections. Each quadrangular pieces of tissue were glued on the tip of resin blocks and cut into 80 nm ultrathin sections with an ultramicrotome (model EM UC7, Leica). Ultrathin sections were collected on bare 150-mesh copper grids and examined under a transmission electron microscope (Tecnai 12; Philips Electronic, Amsterdam, Netherlands) at 100 kV. Profiles of axon varicosities were readily identified as such by their diameter (larger than 0.25 µm) and their synaptic vesicles content. Using an integrated digital camera (MegaView II; Olympus, Münster, Germany), TH immunopositive axon varicosities were imaged randomly, at a working magnification of 9,000X, by acquiring an image of every such profile encountered, until 50 or more showing a full contour and distinct content were available for analysis, in each mouse.

Stereotaxic virus injections

One-month old Nrxn123 KO, Nrxn123 HET and Nrxn123 WT mice were anesthetized with isoflurane (Aerrane; Baxter, Deerfield, IL, USA) and fixed on a stereotaxic frame (Stoelting, Wood Dale, IL, USA). Fur on top of the head was trimmed, and the surgical area was disinfected with iodine alcohol. Throughout the entire procedure, eye gel (Lubrital, CDMV, Canada) was applied to the eyes and a heat pad was placed under the animal to keep it warm. Next, bupivacaine (5-mg/ml and 2-mg/Kg, Marcaine; Hospira, Lake Forest, IL, USA) was subcutaneously injected at the surgical site, an incision of about 1-cm made with a scalpel blade and the cranium was exposed. Using a dental burr, one hole of 1-mm diameter was drilled above the site of injection [AP (anterior-posterior; ML (medial-lateral); DV (dorsal ventral), from bregma]. The following injection coordinates were used: SNc/VTA [AP -3.0 mm; ML ± 0.9 mm; DV -4.3 mm]. Borosilicate pipettes were pulled using a Sutter Instrument, P-2000 puller, coupled to a 10 ul Hamilton syringe (Hamilton, 701 RN) using a RN adaptor (Hamilton, 55750-01) and the whole setup was filled with mineral oil. Using a Quintessential Stereotaxic Injector (Stoelting), solutions to be injected were pulled up in the glass pipette. For expression of ChR2 in DA neurons, 0.1-µl (VTA/SNc) of sterile NaCl containing $4.4x10^{12}$ viral particles/mL of AAV5-EF1a-DIO-hChR2(H134R)-EYFP (UNC GTC Vector Core, NC, USA) was injected. After the unilateral injection, the pipette was left in place for 10-min to allow diffusion and then slowly withdrawn. Finally, the scalp skin was sutured and a subcutaneous injection of the anti-inflammatory drug carprofen (Rimadyl, 50-mg/mL) was given. Animals recovered in their home cage and were closely monitored for 72h. A second dose of carprofen (5-mg/kg) was given if the mice showed evidence of pain.

Electrophysiology and optogenetics

Slice preparation: Mice P70 - 80 (4 weeks post injection) were deeply anesthetized with isoflurane and quickly decapitated. Acute coronal slices (300 µm) were obtained using a vibrating blade

microtome (Leica V1200S) in ice-cold N-Methyl D-Glucamine (NMDG) cutting solution: containing (in mM): 110 NMDG, 20 HEPES, 25 glucose, 30 sodium bicarbonate, 1.25 sodium phosphate, 2.5 potassium chloride, 5 sodium ascorbate, 3 sodium pyruvate, 2 Thiourea, 10 magnesium, 0.5 calcium chloride, 305-310 mOsm, pH 7.4. Slices equilibrated in a homemade chamber for 2 – 3 min (31°C) in the above solution and an additional 60 min in room temperature aCSF containing (in mM): 121 NaCl, 26 NaHCO3, 1 NaH2PO4, 2.5 KCl, 11 Glucose, No Sucrose, 1.3 MgSO4-7 H2O, and 2.5 CaCl2 (pH 7.4) before being transferred to a recording chamber.

Whole-Cell Patch-Clamp: Recordings were obtained from medium spiny neurons (MSNs) in the dorsal and ventral striatum. Striatal MSNs were visualized under IR-DIC. Data were collected with a Multiclamp 700B amplifier, Digidata 1550B (Molecular devices), and using Clampex 11 (pClamp; Molecular Devices, San Jose, CA). All recordings were acquired in voltage clamp (Vh= -70 mV) at 31°C and QX-314 (1uM) was used in all internal solutions to internally block sodium-channels. Whole cell currents were acquired and sampled at 10 kHz with a lowpass bessel filter set at 2 kHz and digitized at 10 kHz. For excitatory currents (EPSCs), the patch pipette was filled with internal solution containing (in mM): 135 CsMeSO4, 8 CsCl, 10 HEPES, 0.25 EGTA, 10 Phosphocreatine, 4 MgATP, and 0.3 NaGTP (295 – 305 mOsm, pH 7.4 with CsOH) and Picrotoxin (50μM) was added to aCSF. For inhibitory postsynaptic currents (IPSC), patch pipettes were filled with internal solution containing (in mM): 143 CsCl, 10 HEPES, 0.25 EGTA, 10 Phosphocreatine, 4 MgATP, and 0.3 Na-2GTP (osmolarity 295 – 305, pH 7.4 with CsOH) and CNQX (50μM) and AP5 (10μM) were added to aCSF. All pipettes (3 - 4 MΩ) were pulled from borosilicate glass (Narishige PC-100). Patched cells were allowed a minimum of 3 min to stabilize following break-in and access resistance (Ra) was monitored throughout the recording and cells with an increase of > 20% in Ra were discarded. Optically evoked synaptic currents were induced with a 440nm wavelength laser delivered through a 40X objective lens (Olympus BX51WI) at 0.1 Hz (5 ms pulse) and laser intensity was adjusted using a LLE-SOLA-SE2 controller (Lumencore). Electrically evoked synaptic currents in MSNs were evoked using a bipolar stimulation electrode placed in the

dorsal or in the ventral striatum to evoked-all-or-none responses using the following parameters: 0.1 Hz frequency, pulse duration 0.1ms. Input/output (I/O) curves were also obtained to compare synaptic strength. I/O curve were performed with a stimulation at a frequency of 0.1Hz with intensity increments of 10µA (starting at 10µA and finishing at 100µA) with 3 sweeps per increment. To examine whether synaptic plasticity was altered in Nrxn123 KO mice, we also performed paired pulse ratio (PPR) experiments. PPR of evoked EPSCs and IPSCs were obtained with 40, 50 and 100ms inter-pulse interval and by dividing the amplitude of the second EPSC or IPSC by the first one (EPSC2/EPSC1 or IPSC2/IPSC1).

Immunohistochemistry on brain slices

Three months old male Nrxn123 WT and Nrxn123 KO mice were anesthetized using pentobarbital NaCl solution (7 mg/mL) injected intraperitoneally and then perfused intracardially with 20 mL of PBS followed by 30 mL of 4% PFA. The brains were extracted, placed in PFA for 48h and then in a 30% sucrose solution for 48h. After this period, brains were frozen in -30°C isopentane for 1 min. 40 microns thick coronal sections were then cut using a cryostat (Leica CM1800) and placed in antifreeze solution at -20°C until used. For slice immunostaining, after a PBS wash, the tissue was permeabilized, nonspecific binding sites were blocked and slices were incubated overnight with a rabbit anti-TH (1:1000, AB152, Millipore Sigma, USA), a mouse anti- TH (1:1000, Clone LNC1, MAB318, Millipore Sigma, USA), a rat anti-DAT (1:2000, MAB369; MilliporeSigma, USA), a rabbit anti-VMAT2 (1:2000, kindly provided by Dr. G.W. Miller, Columbia University) or a chicken anti-GFP (1:1000, GFP-1020; Aves Labs, USA) antibody. Primary antibodies were subsequently detected with rabbit, rat or chicken Alexa Fluor-488–conjugated, 546-conjugated and/or 647-conjugated secondary antibodies (1:500, 2h incubation; Invitrogen). Slices were mounted on charged microscope slides (Superfrost/Plus, Fisher Scientific, Canada) and stored at 4°C prior to image acquisition.

Fast scan cyclic voltammetry

Acute brain slices from 3-months-old Nrxn123 WT, Nrxn123 HET and Nrxn123 KO mice, were used for the Fast Scan Cyclic Voltammetry (FSCV) recordings. The animals were anesthetized with halothane, quickly decapitated and the brain harvested. Next, the brain was submersed in ice-cold oxygenated artificial cerebrospinal fluid (aCSF) containing (in mM): NaCl (125), KCl (2.5), KH2PO4 (0.3), NaHCO3 (26), glucose (10), CaCl2 (2.4), MgSO4 (1.3) and coronal striatal/nucleus accumbens brain slices of 300µm were prepared with a Leica VT1000S vibrating blade microtome. Once sliced, the tissue was transferred to oxygenated aCSF at room temperature and allowed to recover for at least 1h. For recordings, slices were put in a custom-made recording chamber superfused with aCSF at 1 ml/min and maintained at 32°C with a TC-324B single channel heater controller. All solutions were adjusted at pH 7.35-7.4, 300 mOsm/kg and saturated with 95% O_2-5% CO_2 at least 30-min prior experiment. Electrically-evoked action potential-induced DA overflow was measured by FSCV using a 7µm diameter carbon-fiber electrode crafted as previously described (Martel et al., 2011) and placed into the tissue ~100µm below the surface and a bipolar electrode (Plastics One, Roanoke, VA, USA) was placed ~200µm away. The electrodes were calibrated with 1µM DA in aCSF before and after each recorded slice and the mean of the current values obtained were used to determine the amount of released DA. After use, electrodes were cleaned with isopropyl alcohol (Bioshop). The potential of the carbon fiber electrode was scanned at a rate of 300 V/s according to a 10ms triangular voltage wave (−400 to 1000 mV vs Ag/AgCl) with a 100ms sampling interval, using a headstage preamp (Axon instrument, CV 203BU) and a Axopatch 200B amplifier (Axon Instruments, Union City, CA). Data were acquired using a digidata 1440a analog to digital board converter (Axon Instruments) connected to a personal computer using Clampex (Axon Instruments). Slices were left to stabilize for 20-min before any electrochemical recordings. Evaluation of DA release was achieved by sampling 4 different subregions of the dorsal striatum and 4 different subregions of the ventral striatum (nucleus accumbens core and shell) using slices originating from +1.34 to +0.98 using bregma as a reference.

After positioning of the bipolar stimulation and carbon fiber electrodes in the tissue, single pulses (400µA, 1ms) were applied to trigger DA release. After sampling of DA release, per pulse ratio experiments were conducted using one spot of the dorsal striatum and one in the nucleus accumbens core. In each spot, a series of single pulses every 2-min for 10-min was collected as a baseline, follow by a triplicate of single-pulse stimuli intercalated with paired pulses (100 Hz) every 2-min (double pulse of 1ms, 400µA, with an inter-pulse interval of 100ms). DA release was analyzed as the peak height of DA concentrations (rise time) and DA reuptake was determined from the clearance rate of DA which was assumed to follow Michaelis-Menten kinetics. The time constant Tau (t) was used as an uptake parameter and was calculated based on an exponential fitting applied to all traces with a homemade MATLAB script. The paired pulse ratio was calculated using the peak height of the 1^{st} and 2^{nd} pulse as: (2^{nd} pulse - 1^{st}) /1^{st}.

Behavioral testing

Before behavioral experiments, mice were transferred from the colony and were housed with a maximum of 4 mice per cage. All mice were handled for 3 consecutive days prior to start of the different tests. All tests were performed in the same order as described below. The animals were tested between 10:00AM and 4:30PM.

Rotarod: The accelerating rotarod task was used to assess motor coordination and learning. The apparatus consisted of five rotating rods separated by walls and elevated 30 cm from the ground. P60-P70 mice were pre-trained on the rod (LE8205, Harvard apparatus) one day before the recording to reach a stable performance. Mice were required to remain on the rod for 1-min at a constant speed of 4rpm with a maximum of 3 attempts. For the first step of the rotarod testing protocol, the first day of the data acquisition, mice were tested on an accelerated rotation 4-40rpm over a 10-min period for two sessions with an interval of 1h. The latency to fall was recorded. The same parameters were used on the second test day, but 3 sessions were performed. On the last day of data acquisition, the mice performed 4 sessions with the same previous parameters. A second

protocol was also used, in which mice were tested with an accelerated rotation 4-40rpm over a 2-min period for all sessions with an interval of 1h. Each trial per day was analyzed separately and compared between the genotypes.

Locomotor activity and psychostimulant-induced locomotor activity: To evaluate motor behavior, mice were placed in cages (Omnitech Electronics, Inc; USA) designed for activity monitoring using an infrared actimeter (Superflex sensor version 4.6, Omnitech Electronics; 40 x 40 x 30cm) for 20-min. Next, 0.9% saline or the drug treatments were injected intraperitoneally (10ml/kg) in a randomized order for the different genotypes. Horizontal activity was scored for 40-min following the injection. To evaluate psychostimulant-induced motor behaviors, the mice were placed in the infrared actimeter cages (Superflex sensor version 4.6, Omnitech Electronics) for 20-min. Then, amphetamine was injected intraperitoneally at 5-mg/kg (Tocris, UK) or cocaine hydrochloride at 20-mg/Kg (Medisca, cat# 53-21-4, Canada) in a randomized order for the different genotypes. The total distance (horizontal locomotor activity) was scored for 40-min following the injection.

Pole test: The test was conducted with a homemade 48-cm metal rod of 1-cm diameter covered with adhesive tape to facilitate traction, placed in a cage. 8-week-old Nrxn123 KO, HET and WT mice were positioned head-up at the top of the pole and the time required to turn (t-turn) and climb down completely was recorded.

Sucrose preference test: Mice were tested for preference of a 2% sucrose solution, using a two bottles choice procedure. Subjects were housed one per cage all of the test (5 days). Mice were first conditioned with two bottles of water during two days. Then mice were given two bottles, one sucrose (2%) and one of tap water. Every 24h, the amount of sucrose and water consumed was evaluated. To prevent potential location preference of drinking, the position of the bottles was changed every 24h. The preference for the sucrose solution was calculated as the percentage of sucrose solution ingested relative to the total intake.

Reverse transcription quantitative polymerase chain reaction (RT-qPCR)

We used RT-qPCR to quantify the amount of mRNA encoding the following genes: gephyrin (Gphn), collybistin (Arhgef 9), GABA-A receptor (Gabra1), neuroligins 1, 2 and 3 (Nlgn1, 2 and3), latrophilins 1, 2 and 3 (Lphn1, 2 and 3), LRRTMs 1, 2, 3, 4 (LRRTM1, 2, 3 and 4), D1R (DRD1) and D2R (DRD2) in striatal brain tissue from P80 Nrxn123 WT and Nrxn123 KO mice. The brains were quickly harvested and the ventral and dorsal striata were microdissected and homogenized in 500 µL of trizol. For both, presynaptic and postsynaptic compartment, RNA extraction was performed using RNAeasy Mini Kit (Qiagen, Canada) according to the manufacturer's instructions. RNA integrity was validated using a Bioanalyzer 2100 (Agilent). Total RNA was treated with DNase and reverse transcribed using the Maxima First Strand cDNA synthesis kit with ds DNase (Thermo Fisher Scientific). Gene expression was determined using assays designed with the Universal Probe Library from Roche (www.universalprobelibrary.com). For each qPCR assay, a standard curve was performed to ensure that the efficiency of the assay was between 90% and 110%. Assay information are presented in **supplementary Table 1**. The Quant Studio qPCR instrument (Thermo Fisher Scientific) was used to detect the amplification level. Relative expression comparison ($RQ = 2^{\wedge -\Delta\Delta CT}$) was calculated using the Expression Suite software (Thermo Fisher Scientific), using GAPDH and β-Actin as an endogenous control.

Western Blot

Ventral and dorsal striatum samples were microdissected from Nrxn123 WT and Nrxn123 KO adult mice and then lysed in RIPA buffer (Fisher Scientific, PI89900) containing a protease inhibitor cocktail (P840, Sigma). Homogenized tissue samples were centrifuged at 12000g for 30 min at 40C. Supernatant was collected, and protein quantification was done with BCA reagent (Thermo Scientific Pierce BCA Protein Assay Kit, PI23227). 20µg of each sample was separated on 8% SDS-PAGE followed by transfer onto a nitrocellulose membrane. Membrane blocking was done with 10% skimmed milk for 90 min at RT with gentle shaking. The membranes were incubated overnight at 4°C with respective antibodies (**Supplementary Table 2**) with gentle

shaking. Membranes were washed 5 times with TBST buffer for 5 min each time. After this, appropriate secondary antibodies (**Supplementary Table 2**) were added, and the incubation was performed at RT for 90 min with gentle shaking. Membranes were washed again with TBST buffer for 5 times X 5 min and developed using the Clarity Western ECL substrate (Bio-Rad, 1004384863). Images were captured on a luminescent image analyzer (GE Healthcare) using Image quant LAS 4000 software. Membranes were stripped and re-probed for β-actin as a loading control.

Image acquisition with confocal microscopy

All *in vitro* fluorescence imaging quantification analyses were performed on images acquired using an Olympus Fluoview FV1000 point-scanning confocal microscope (Olympus, Tokyo, Japan). Images were scanned sequentially to prevent non-specific bleed-through signal using 488, 546 and 647-nm laser excitation and a 60X (NA 1:42) oil immersion objective.

Image analysis

All image quantification was performed using Image-J (National Institute of Health, NIH) software. A background correction was first applied at the same level for every image analyzed before any quantification. A macro developed in-house was used to perform all quantifications.

Statistics

Data are represented throughout as mean ± SEM. Statistically significant differences were analyzed using Student's t test, one-way repeated-measures ANOVA or two-way ANOVA with Tukey's or Sidak's multiple comparison test (*$p < 0.05$; **$p < 0.01$; ***$p < 0.001$; ****$p < 0.0001$).

Acknowledgments

We would like to thank Dr. G. Miller for kindly provided VMAT2 antibody, Willemieke Kouwenhoven for her help with some experiments, the IRIC genomic platform for qRT-PCR analysis, CERVO Québec electron microscopy platform and C.A. Maurice for his strong support. This work was funded by Canadian Institutes of Health Research (CIHR, grant MOP106556) to L-E.T. C.D. received a graduate student award from Fond de recherche en santé du Québec (FRQS).

Author contributions

C.D.: conceptualization, design, acquisition, analysis, validation and interpretation of data (All *in vitro* results, ICC, GABA uptake, Behavior, IHC, qRT-PCR, Transmission electron microscopy, TEM), drafting, revising and editing the manuscript. G. D. C: acquisition of data and analysis (Whole cell patch clamp recording). C. VL. D.: acquisition of TEM. S.M.: acquisition and analysis of data (Western Blot). N.G.: viral injections. S.B.N.: help with data analysis (ICC). M-J.: acquisition of data (cell culture), B. D. L.: acquisition of data and analysis (voltammetry). L. Y. C.: providing Nrxn123flox/flox mice, genotyping and injection verification, electrophysiology analysis, conceptualization, writing, and review and editing. L-E.T.: conceptualization, resources, funding acquisition, writing, review and editing.

Declaration of interests

The authors declare no conflicts of interests.

References

Aoto J, Foldy C, Ilcus SM, Tabuchi K, Sudhof TC (2015) Distinct circuit-dependent functions of presynaptic neurexin-3 at GABAergic and glutamatergic synapses. Nat Neurosci 18:997-1007.

Banerjee A, Lee J, Nemcova P, Liu C, Kaeser PS (2020) Synaptotagmin-1 is the Ca(2+) sensor for fast striatal dopamine release. Elife 9.

Berube-Carriere N, Guay G, Fortin GM, Kullander K, Olson L, Wallen-Mackenzie A, Trudeau LE, Descarries L (2012) Ultrastructural characterization of the mesostriatal dopamine innervation in mice, including two mouse lines of conditional VGLUT2 knockout in dopamine neurons. Eur J Neurosci 35:527-538.

Birgner C, Nordenankar K, Lundblad M, Mendez JA, Smith C, le Greves M, Galter D, Olson L, Fredriksson A, Trudeau LE, Kullander K, Wallen-Mackenzie A (2010) VGLUT2 in dopamine neurons is required for psychostimulant-induced behavioral activation. Proc Natl Acad Sci U S A 107:389-394.

Caille I, Dumartin B, Bloch B (1996) Ultrastructural localization of D1 dopamine receptor immunoreactivity in rat striatonigral neurons and its relation with dopaminergic innervation. Brain Res 730:17-31.

Chen LY, Jiang M, Zhang B, Gokce O, Sudhof TC (2017) Conditional Deletion of All Neurexins Defines Diversity of Essential Synaptic Organizer Functions for Neurexins. Neuron 94:611-625 e614.

Condon MD, Platt NJ, Zhang YF, Roberts BM, Clements MA, Vietti-Michelina S, Tseu MY, Brimblecombe KR, Threlfell S, Mann EO, Cragg SJ (2019) Plasticity in striatal dopamine release is governed by release-independent depression and the dopamine transporter. Nat Commun 10:4263.

Craig AM, Banker G, Chang W, McGrath ME, Serpinskaya AS (1996) Clustering of gephyrin at GABAergic but not glutamatergic synapses in cultured rat hippocampal neurons. J Neurosci 16:3166-3177.

Dal Bo G, St-Gelais F, Danik M, Williams S, Cotton M, Trudeau LE (2004) Dopamine neurons in culture express VGLUT2 explaining their capacity to release glutamate at synapses in addition to dopamine. J Neurochem 88:1398-1405.

Dal Bo G, Berube-Carriere N, Mendez JA, Leo D, Riad M, Descarries L, Levesque D, Trudeau LE (2008) Enhanced glutamatergic phenotype of mesencephalic dopamine neurons after neonatal 6-hydroxydopamine lesion. Neuroscience 156:59-70.

Delignat-Lavaud B, Kano J, Ducrot C, Massé I, Mukherjee S, Giguère N, Moquin L, Lévesque C, Nanni SB, Bourque M-J, Rosa-Neto P, Lévesque D, De Beaumont L, Trudeau L-É (2021) The calcium sensor synaptotagmin-1 is critical for phasic axonal dopamine release in the striatum and mesencephalon, but is dispensable for basic motor behaviors in mice. bioRxiv:2021.2009.2015.460511.

Descarries L, Mechawar N (2000) Ultrastructural evidence for diffuse transmission by monoamine and acetylcholine neurons of the central nervous system. Prog Brain Res 125:27-47.

Descarries L, Bosler O, Berthelet F, Des Rosiers MH (1980) Dopaminergic nerve endings visualised by high-resolution autoradiography in adult rat neostriatum. Nature 284:620-622.

Descarries L, Watkins KC, Garcia S, Bosler O, Doucet G (1996) Dual character, asynaptic and synaptic, of the dopamine innervation in adult rat neostriatum: a quantitative autoradiographic and immunocytochemical analysis. J Comp Neurol 375:167-186.

Descarries L, Berube-Carriere N, Riad M, Bo GD, Mendez JA, Trudeau LE (2008) Glutamate in dopamine neurons: synaptic versus diffuse transmission. Brain Res Rev 58:290-302.

Di Chiara G, Imperato A (1988) Drugs abused by humans preferentially increase synaptic dopamine concentrations in the mesolimbic system of freely moving rats. Proc Natl Acad Sci U S A 85:5274-5278.

Ducrot C, Bourque MJ, Delmas CVL, Racine AS, Guadarrama Bello D, Delignat-Lavaud B, Domenic Lycas M, Fallon A, Michaud-Tardif C, Burke Nanni S, Herborg F, Gether U, Nanci A, Takahashi H, Parent M, Trudeau LE (2021) Dopaminergic neurons establish a distinctive axonal arbor with a majority of non-synaptic terminals. FASEB J 35:e21791.

Etherton MR, Blaiss CA, Powell CM, Sudhof TC (2009) Mouse neurexin-1alpha deletion causes correlated electrophysiological and behavioral changes consistent with cognitive impairments. Proc Natl Acad Sci U S A 106:17998-18003.

Fasano C, Thibault D, Trudeau LE (2008) Culture of postnatal mesencephalic dopamine neurons on an astrocyte monolayer. Curr Protoc Neurosci Chapter 3:Unit 3 21.

Gerfen CR, Surmeier DJ (2011) Modulation of striatal projection systems by dopamine. Annu Rev Neurosci 34:441-466.

Graf ER, Zhang X, Jin SX, Linhoff MW, Craig AM (2004) Neurexins induce differentiation of GABA and glutamate postsynaptic specializations via neuroligins. Cell 119:1013-1026.

Hata Y, Butz S, Sudhof TC (1996) CASK: a novel dlg/PSD95 homolog with an N-terminal calmodulin-dependent protein kinase domain identified by interaction with neurexins. J Neurosci 16:2488-2494.

Ichtchenko K, Hata Y, Nguyen T, Ullrich B, Missler M, Moomaw C, Sudhof TC (1995) Neuroligin 1: a splice site-specific ligand for beta-neurexins. Cell 81:435-443.

Ko J, Fuccillo MV, Malenka RC, Sudhof TC (2009) LRRTM2 functions as a neurexin ligand in promoting excitatory synapse formation. Neuron 64:791-798.

Kornau HC, Seeburg PH, Kennedy MB (1997) Interaction of ion channels and receptors with PDZ domain proteins. Curr Opin Neurobiol 7:368-373.

Li J, Ashley J, Budnik V, Bhat MA (2007) Crucial role of Drosophila neurexin in proper active zone apposition to postsynaptic densities, synaptic growth, and synaptic transmission. Neuron 55:741-755.

Liu C, Kershberg L, Wang J, Schneeberger S, Kaeser PS (2018) Dopamine Secretion Is Mediated by Sparse Active Zone-like Release Sites. Cell 172:706-718 e715.

Luo F, Sclip A, Jiang M, Sudhof TC (2020) Neurexins cluster Ca(2+) channels within the presynaptic active zone. EMBO J 39:e103208.

Luo F, Sclip A, Merrill S, Sudhof TC (2021) Neurexins regulate presynaptic GABAB-receptors at central synapses. Nat Commun 12:2380.

Martel P, Leo D, Fulton S, Berard M, Trudeau LE (2011) Role of Kv1 potassium channels in regulating dopamine release and presynaptic D2 receptor function. PLoS One 6:e20402.

Matsuda W, Furuta T, Nakamura KC, Hioki H, Fujiyama F, Arai R, Kaneko T (2009) Single nigrostriatal dopaminergic neurons form widely spread and highly dense axonal arborizations in the neostriatum. J Neurosci 29:444-453.

Mendez JA, Bourque MJ, Dal Bo G, Bourdeau ML, Danik M, Williams S, Lacaille JC, Trudeau LE (2008) Developmental and target-dependent regulation of vesicular glutamate transporter expression by dopamine neurons. J Neurosci 28:6309-6318.

Missler M, Zhang W, Rohlmann A, Kattenstroth G, Hammer RE, Gottmann K, Sudhof TC (2003) Alpha-neurexins couple Ca2+ channels to synaptic vesicle exocytosis. Nature 423:939-948.

Ogura T, Ogata M, Akita H, Jitsuki S, Akiba L, Noda K, Hoka S, Saji M (2005) Impaired acquisition of skilled behavior in rotarod task by moderate depletion of striatal dopamine in a pre-symptomatic stage model of Parkinson's disease. Neurosci Res 51:299-308.

Robinson BG, Cai X, Wang J, Bunzow JR, Williams JT, Kaeser PS (2019) RIM is essential for stimulated but not spontaneous somatodendritic dopamine release in the midbrain. Elife 8.

Sanchez G, Varaschin RK, Bueler H, Marcogliese PC, Park DS, Trudeau LE (2014) Unaltered striatal dopamine release levels in young Parkin knockout, Pink1 knockout, DJ-1 knockout and LRRK2 R1441G transgenic mice. PLoS One 9:e94826.

Schultz W (2007) Multiple dopamine functions at different time courses. Annu Rev Neurosci 30:259-288.

Stuber GD, Hnasko TS, Britt JP, Edwards RH, Bonci A (2010) Dopaminergic terminals in the nucleus accumbens but not the dorsal striatum corelease glutamate. J Neurosci 30:8229-8233.

Sulzer D, Joyce MP, Lin L, Geldwert D, Haber SN, Hattori T, Rayport S (1998) Dopamine neurons make glutamatergic synapses in vitro. J Neurosci 18:4588-4602.

Surmeier DJ, Graves SM, Shen W (2014) Dopaminergic modulation of striatal networks in health and Parkinson's disease. Curr Opin Neurobiol 29:109-117.

Tabuchi K, Sudhof TC (2002) Structure and evolution of neurexin genes: insight into the mechanism of alternative splicing. Genomics 79:849-859.

Tritsch NX, Ding JB, Sabatini BL (2012) Dopaminergic neurons inhibit striatal output through non-canonical release of GABA. Nature 490:262-266.

Tritsch NX, Granger AJ, Sabatini BL (2016) Mechanisms and functions of GABA co-release. Nat Rev Neurosci 17:139-145.

Tritsch NX, Oh WJ, Gu C, Sabatini BL (2014) Midbrain dopamine neurons sustain inhibitory transmission using plasma membrane uptake of GABA, not synthesis. Elife 3:e01936.

Ullrich B, Ushkaryov YA, Sudhof TC (1995) Cartography of neurexins: more than 1000 isoforms generated by alternative splicing and expressed in distinct subsets of neurons. Neuron 14:497-507.

Ushkaryov YA, Petrenko AG, Geppert M, Sudhof TC (1992) Neurexins: synaptic cell surface proteins related to the alpha-latrotoxin receptor and laminin. Science 257:50-56.

Wang A, Xiang YY, Yang BB, Lu WY (2019) Neurexin-1alpha regulates neurite growth of rat hippocampal neurons. Int J Physiol Pathophysiol Pharmacol 11:115-125.

Yorgason JT, Espana RA, Jones SR (2011) Demon voltammetry and analysis software: analysis of cocaine-induced alterations in dopamine signaling using multiple kinetic measures. J Neurosci Methods 202:158-164.

Zhang H, Sulzer D (2004) Frequency-dependent modulation of dopamine release by nicotine. Nat Neurosci 7:581-582.

Zhou QY, Palmiter RD (1995) Dopamine-deficient mice are severely hypoactive, adipsic, and aphagic. Cell 83:1197-1209.

Figures and figures legends

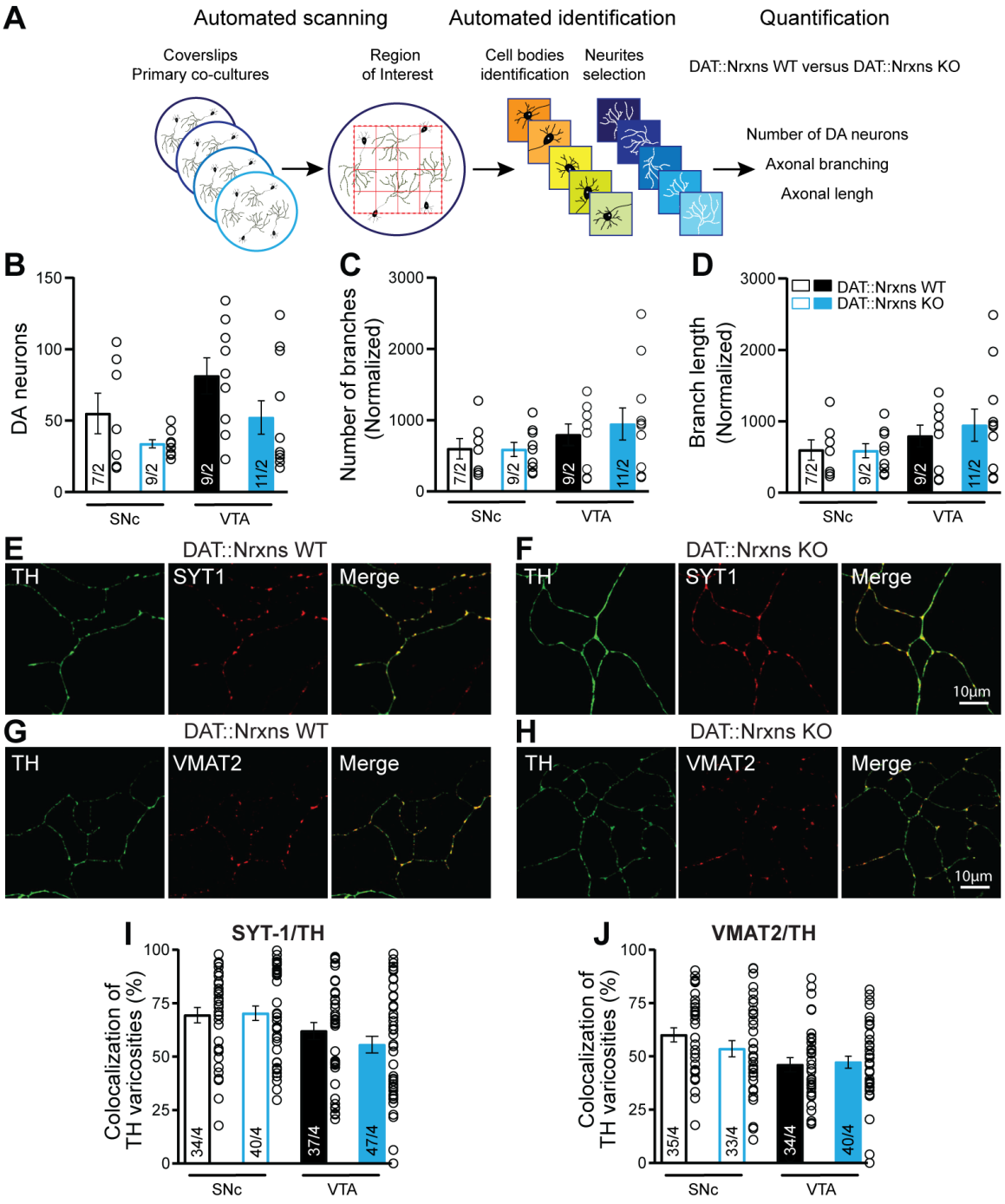

Figure 1 – Normal axonal growth in DA neurons after conditional deletion of all neurexins. **A** - Illustration of the method used to evaluate and quantify the survival and growth of DA neurons lacking all neurexins. **B** - Quantification of DA neuron survival, assessed by their number per coverslip at 14DIV (SNc WT=55.00 ± 14.18; SNc KO=33.78 ± 2.84; VTA WT=81.33 ± 12.62; VTA KO=52.18 ± 11.72). **C** and **D** - Evaluation of neurite development in cultured DA neurons, assessed by quantifying the number of TH-positive processes (**C**) and their length (**D**) (*Branch length*: SNc WT= 19086 ± 1749µm, SNc KO= 14950 ± 2068 µm, VTA WT= 34721 ± 9282 µm, VTA KO= 30593 ± 4715 µm, Two-way ANOVA, p=0.47*; Branch number*: SNc WT= 598.9 ± 143.3, SNc KO= 588.2 ± 99.37, VTA WT= 795.4 ± 152.6, VTA KO= 945.7 ± 225.7). **E and F**- Photomicrographs illustrating the distribution of TH/Syt-1 positive axonal varicosities along the axonal domain of a SNc DA neuron from DAT::NrxnsWT and DAT::NrxnsKO mice. **G and H**- Photomicrographs illustrating the distribution of TH/VMAT2 positive axonal varicosities along the axonal domain of a SNc DA neuron from DAT::NrxnsWT and DAT::NrxnsKO mice. **I**- Summary graph showing the proportion of TH-positive terminals containing Syt1. **J**- Summary graph showing the proportion of TH-positive terminals containing VMAT2. For axonal growth assessment: n = 7-11 coverslips from 2 different neuronal co-cultures. For Syt1/VMAT2 quantifications: n = 33-44 axonal fields from 4 different neuronal co-cultures. The number of observations represent the number of fields from individual neuronal examined. For all analyses, the plots represent the mean ± SEM. Statistical analysis was carried out by 2-way ANOVAs followed by Šidák's corrections (*p < 0.05; **p < 0.01; ***p < 0.001; ****p < 0.0001).

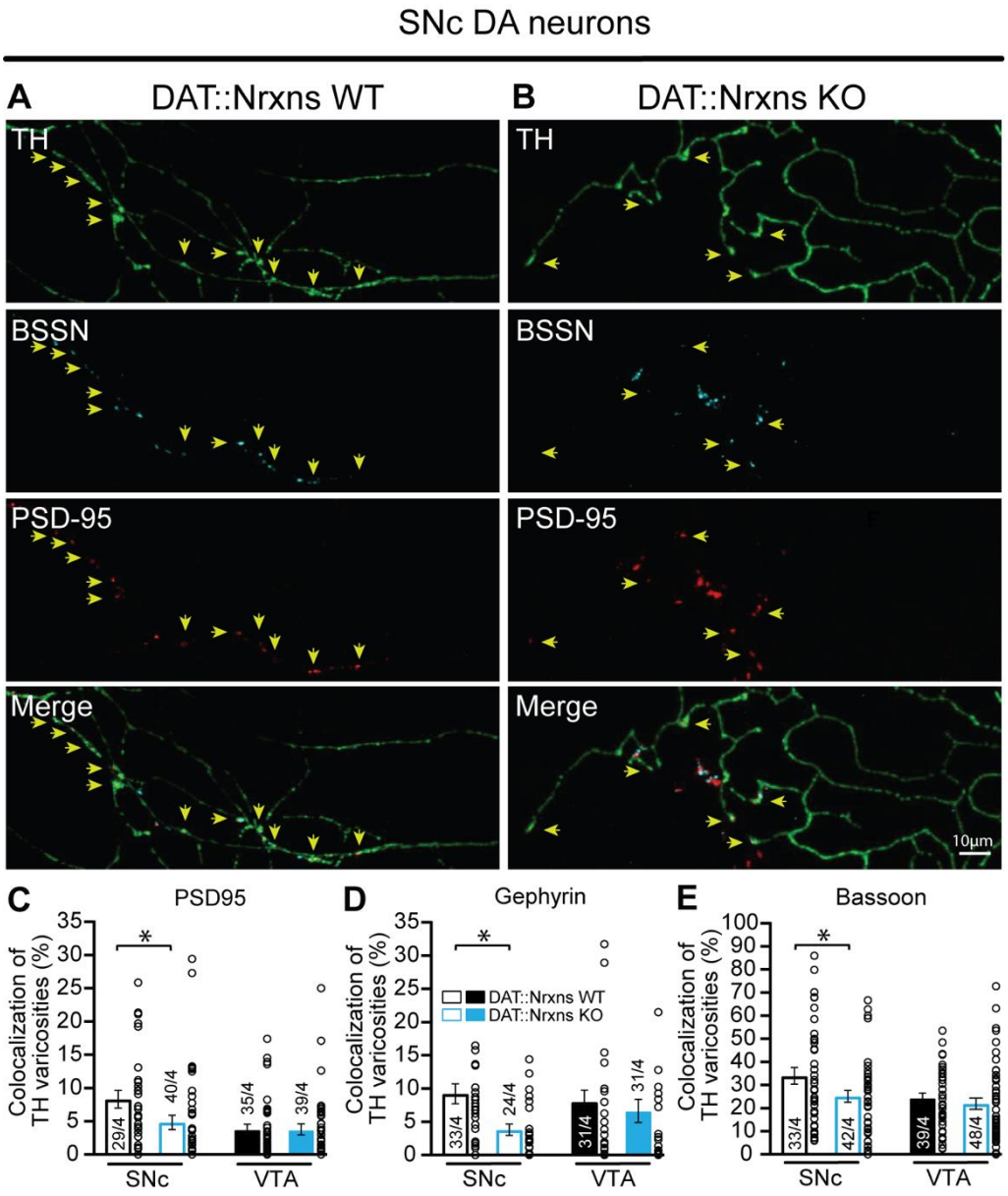

Figure 2 – The proportion of synapses established by cultured SNc DA neurons is reduced after conditional deletion of all neurexins. A and B- Representative images illustrating TH-positive varicosities in the axonal arbor of a SNc DA neuron from DAT::NrxnsWT and DAT::NrxnsKO mice. Bassoon was expressed sparsely and colocalized with the postsynaptic marker PSD95. **C-** Bar graph representing the proportion (%) of axonal varicosities established by VTA and SNc DA neurons that are positive for TH and colocalizing with PSD95 at 14 DIV. **D-** Bar graph representing the proportion (%) of axonal varicosities established by VTA and SNc DA

neurons that are positive for TH and colocalizing with gephyrin at 14 DIV. **E** - Bar graph representing the proportion (%) of axonal varicosities that are positive for bassoon in VTA and SNc DA neurons from DAT::NrxnsWT and DAT::NrxnsKO mice. Data represent mean ± SEM. Statistical analyses were performed by two-tailed Student's T-tests (*p<0.05; ** p<0.01; *** p<0.001).

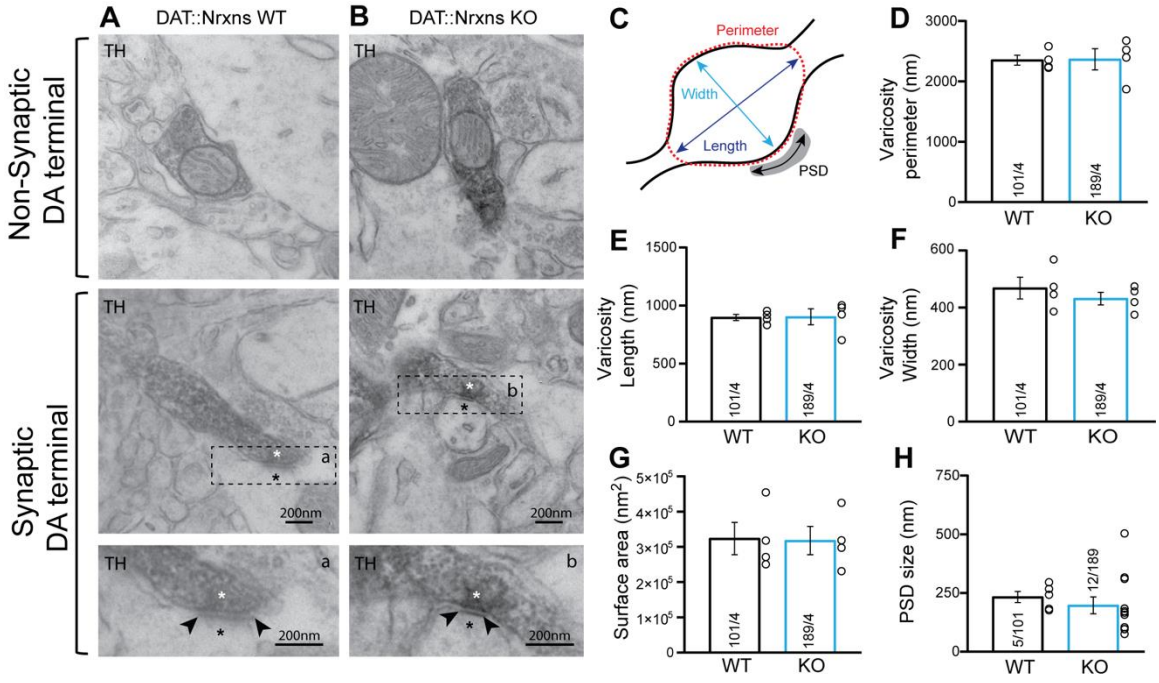

Figure 3 - Synaptic and non-synaptic ultrastructure of DA terminals is unchanged after Nrxn123 triple knockout in dopamine neurons. A-B Electron micrographs showing DA neuron terminals without any PSD domain (top images) or in apposition to a PSD domain in ventral striatal tissue from DAT::NrxnsWT and KO mice. **C**- Schematic representation of a dopaminergic varicosity. **D**- Bar graph representing the perimeter of the DA neuron varicosity from WT and KO mice (2227 ± 81.83 nm and 1870 ± 174.8 nm, respectively), **E** and **F**- Bar graphs representing the size of the axonal varicosities, quantified as length (**E**) (897.3 ± 38.06 nm and 902.7 ± 38.06 nm respectively) and width (**F**) (468.7 ± 38.06 nm and 375.2 ± 22.02 nm, respectively). **G**- Bar graphs

showing the surface area of DA neuron varicosities from WT and KO animals (323537 ± 45861 nm^2 and 317887 ± 40227 nm^2, respectively,). **H-** Bar graphs representing the PSD domain size (232.8 ± 23.40 nm and 197.1 ± 35.71 nm, respectively for WT and KO mice). For all analyses, WT=101 and KO=189 axonal varicosities from 4 different mice for each genotype. For all analyses, plots represent the mean ± SEM. Statistical analyses were carried out by unpaired t-tests (*p < 0.05; **p < 0.01; ***p < 0.001; ****p < 0.0001).

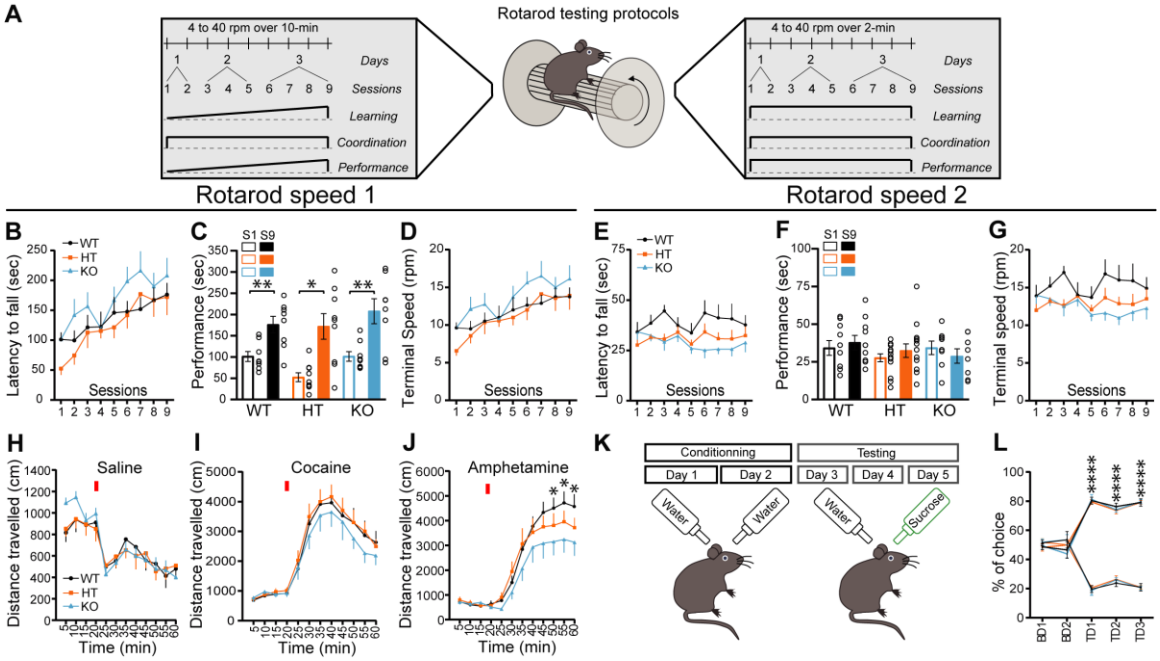

Figure 4 – DAT::NrxnsKO mice exhibit impaired amphetamine-induced motor activity. A- Schematic representation of a mouse on a rotarod and the diagram of the two rotarod testing protocols. **B-** Performance on the accelerating rotarod during 9 sessions over 3 consecutive days. Latency to fall was quantified at rotation speeds from 4 to 40 rpm over 10-min. **C-** Performance of DAT::NrxnsKO, HET and WT littermate mice on the rotarod were evaluated comparing the last session and the first session for each mouse. The results show a significant improvement in performance irrespective of genotype. **D-** Quantification of the terminal speed over all the sessions

shows no difference between the DAT::NrxnsKO, HET and WT littermate mice. **E**- Performance on the second accelerating rotarod task during 9 sessions over 3 consecutive days. Latency to fall was quantified at rotation speeds from 4 to 40 rpm over 2-min. **F**- Performance of DAT::NrxnsWT, HET and KO littermate mice on the rotarod was evaluated comparing the last and first sessions for each mouse. No significant improvement in performance was detected, irrespective of genotype. **G**- Quantification of the final speed over all sessions shows no difference between the DAT::NrxnsWT, HET and KO littermate mice**. H**- Basal horizontal activity in a novel environment before and after a saline injection (10ml/kg) over a total of 60-min. **I**- Horizontal activity before and after a cocaine injection (20mg/kg; 10ml/kg) over a total of 60-min. **J**- Horizontal activity before and after an amphetamine injection (5mg/kg; 10ml/kg) over 60-min, shows reduced locomotion in the DAT::NrxnsKO compared to the control mice. **K**-Schematic representation of the sucrose preference testing protocol. **L**- Quantification of sucrose preference in comparison to water consumption represented as a percentage. Initial two days: DAT::NrxnsKO CD1: 51.87 ± 2.25% vs 49.36 ± 2.38% and CD2: 53.59 ± 3.55%, vs 43.85 ± 2.76%; DAT::NrxnsHET CD1: 51.65 ± 2.57% vs 48.34 ± 2.38% and CD2: 50.07 ± 3.40%, vs 49.92 ± 3.40%; DAT::NrxnsWT CD1: 51.87 ± 2.25% vs 49.36 ± 2.38% and CD2: 53.59 ± 3.55%, vs 43.85 ± 2.76%. Results are presented as the percentage of choice water/water. Following three test days: DAT::NrxnsKO TD1: 81.25 ± 3.33% vs 18.75 ± 3.33%; TD2: 53.59 ± 3.55%, vs 43.85 ± 2.76% and TD2: 53.59 ± 3.55%, vs 43.85 ± 2.76%; DAT::NrxnsHET TD1: 79.34 ± 1.63% vs 20.65 ± 1.63%; TD2: 73.63 ± 2.35%, vs 26.36 ± 2.35% and TD3: 79.16 ± 1.30% vs 20.83 ± 1.30%; DAT::NrxnsWT TD1: 51.87 ± 2.25% vs 49.36 ± 2.38%; TD2: 53.59 ± 3.55%, vs 43.85 ± 2.76% and TD3: 53.59 ± 3.55%, vs 43.85 ± 2.76%). All results are presented as the percentage of choice Sucrose/Water; WT n=6; HET n=6 and TKO n=6 mice). For all analyses, the plots represent the mean ± SEM. Statistical analyses were carried out by 2-way ANOVAs followed by Tukey's multiple comparisons tests (*$p < 0.05$; **$p < 0.01$; ***$p < 0.001$; ****$p < 0.0001$).

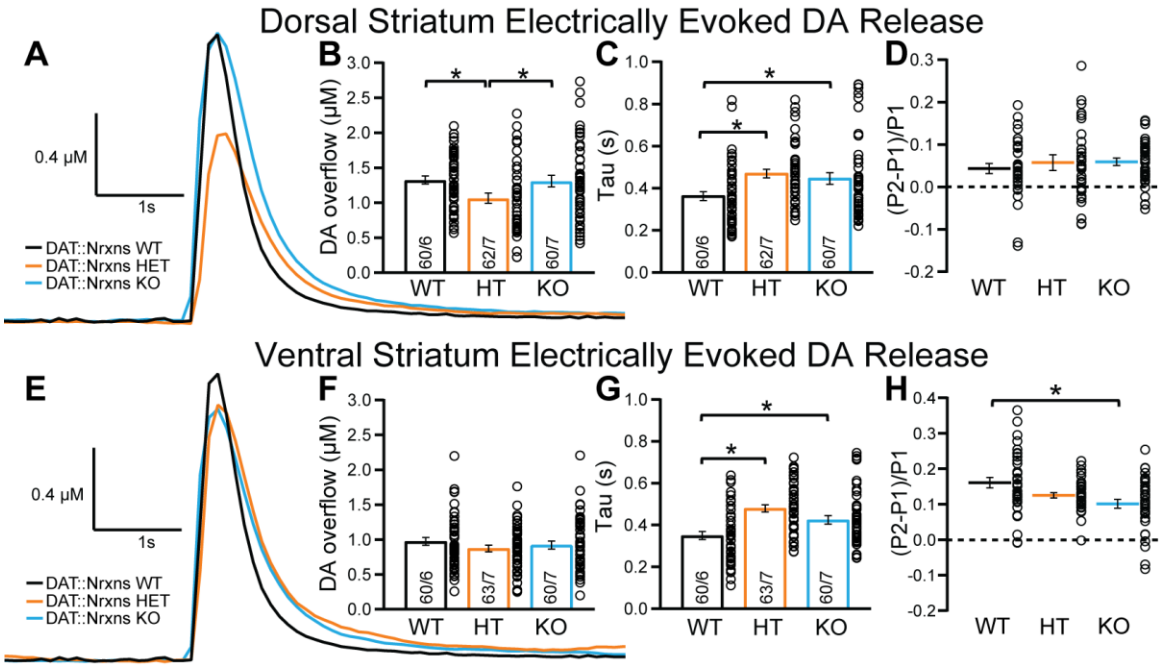

Figure 5 - Normal dopamine release but slower reuptake in DAT::NrxnsKO mice. A- Representative traces of electrically evoked DA levels detected by fast-scan cyclic voltammetry in the dorsal striatum, measured in slices prepared from DAT::NrxnsWT, HET and KO mice. **B**- Bar graphs showing the average DA levels (µM) detected in the dorsal striatum. **C**- Evaluation of DA release kinetics in the dorsal striatum estimated by quantifying Tau, corresponding to reuptake efficiency. **D**- Short-term paired-pulse induced plasticity of DA overflow in dorsal striatal slices, estimated by calculating (P2-P1/P1) with an inter-pulse interval of 100 ms. The low ratio values reflect the strong paired-pulse depression seen at such release sites in acute brain slices. **E**- Representative traces of electrically evoked DA levels detected by fast-scan cyclic voltammetry in the ventral striatum. **F**- Bar graphs showing the average of DA levels (µM) detected in the ventral striatum. **G**- Evaluation of DA release kinetics in the ventral striatum, estimated by quantifying Tau. **H**- Short-term paired-pulse induced plasticity of DA overflow in ventral striatal slices,

estimated by calculating (P2-P1/P1) with an inter-pulse interval at 100-ms. The low ratio values reflect the strong paired-pulse depression seen at such release sites in acute brain slices. Data are presented as mean ± SEM. Statistical analyses were performed with a one-way ANOVA (*p<0.05; ** p<0.01; *** p<0.001).

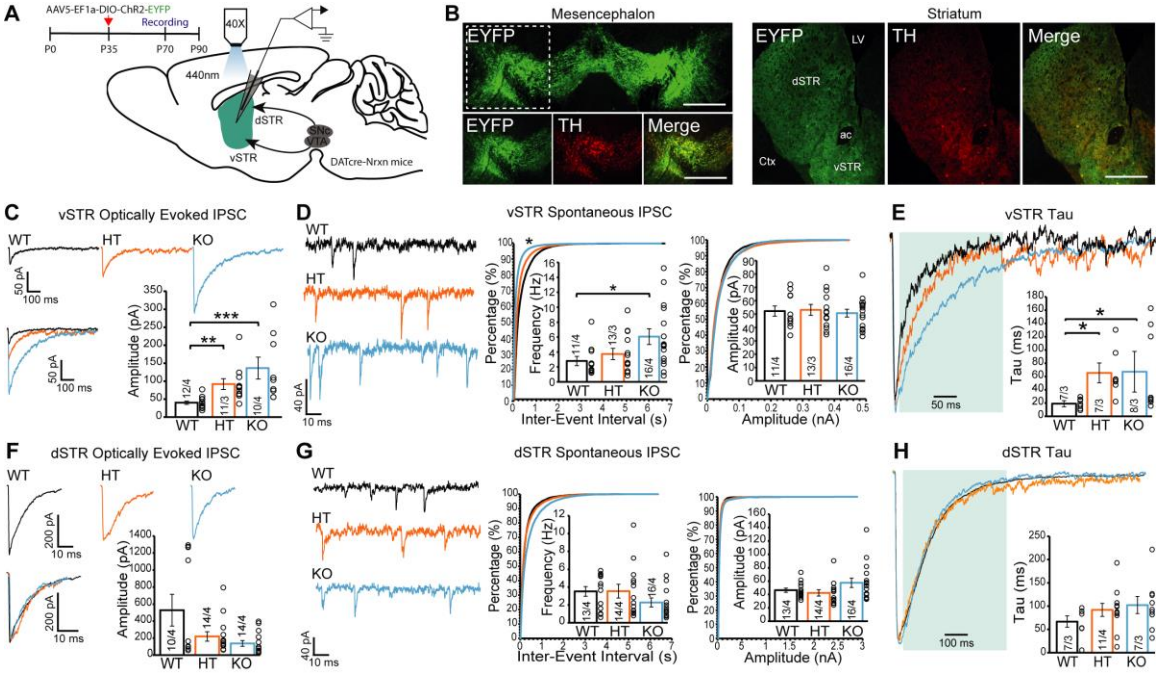

Figure 6 - Neurexins regulate GABA release from dopaminergic neurons in the ventral striatum. A- Schematic representation of the experimental approach used for electrophysiological recordings; The green color represents the EYFP expression reporting ChR2 expression after AAV-transfection of the VTA. **B-** Photomicrographs illustrating the expression of EYFP-ChR2 in TH-positive (red) DA neurons located in the mesencephalon and their projections in the striatum. **C-** Representative traces (top) of IPSCs elicited by optical stimulation (o-IPSC) and recorded in medium spiny neurons (MSNs) of acute ventral striatal slices from WT, HT or KO mice. Summary graph of o-IPSC amplitude (bottom) shows a significant genotype effect (WT vs. HT: **p= 0.0017;

WT vs. KO: ***p= 0.0001) (*Peak Amplitude:* WT = -40.02 ± 4.7 pA, HT = -91.99 ± 14.9 pA, KO = -136.32 ± 30.62, Mean ± SEM.). **D-** Representative traces (left) of spontaneous IPSCs (sIPSC) recorded in ventral striatal MSNs. Cumulative distribution plots of sIPSC inter-event intervals (middle, WT vs. KO: *p= 0.038) and amplitudes (right); insets: summary graphs of average sIPSC frequency (middle, WT vs. KO: *p=0.04) (*sIPSC frequency*, WT = 2.79 ± 0.61 Hz, HT = 3.72 ± 0.74 Hz, KO = 6.06 ± 1.04 Hz, Mean ± SEM) and amplitude (right). **E -** Representative traces and summary graph of o-IPSC decay time in ventral striatal MSNs, showing an increase in time to return to baseline (oIPSC, decay time (90% - 10%): WT = 13.8 ± 2.5 ms, HT = 31.6 ± 4.2 ms, KO = 36.2 ± 8.3 ms, Mean ± SEM). **F -**Representative traces (left) of o-IPSCs recorded in MSNs of acute dorsal striatal slices from WT, HT or KO mice. The summary graph of o-IPSC amplitude (bottom) shows no genotype effect (Peak Amplitude: WT = -528.50 ± 187.31 pA, HT = -219.68 ± 54.87 pA, KO = -138.03 ± 34.57, Mean ± SEM). **G**- Representative traces (left) of sIPSCs recorded in dorsal striatal MSNs. Cumulative distribution plots of sIPSC inter-event intervals (middle) and amplitudes (right); insets: summary graphs of average sIPSC frequency (middle) and amplitude (right). Summary graphs show no genotype effect **H-** Representative traces and summary graph of o-IPSC decay time in dorsal striatal MSNs shows no change in tau for both HT and KO compared to the WT group. Data in summary graphs are presented as mean ± SEM; statistical comparisons were performed with One-Way ANOVA (*P<0.05; **P<0.01; ***P<0.001; non-significant comparisons are not identified). Tukey's correction was used for all multiple comparisons. The Kruskal-Wallis non-parametric test was used to compare cumulative distributions in **D** and **G**. Numbers in bars indicate the number of cells/mice. Each open circle in the summary graphs represent the averaged recording of each cell.

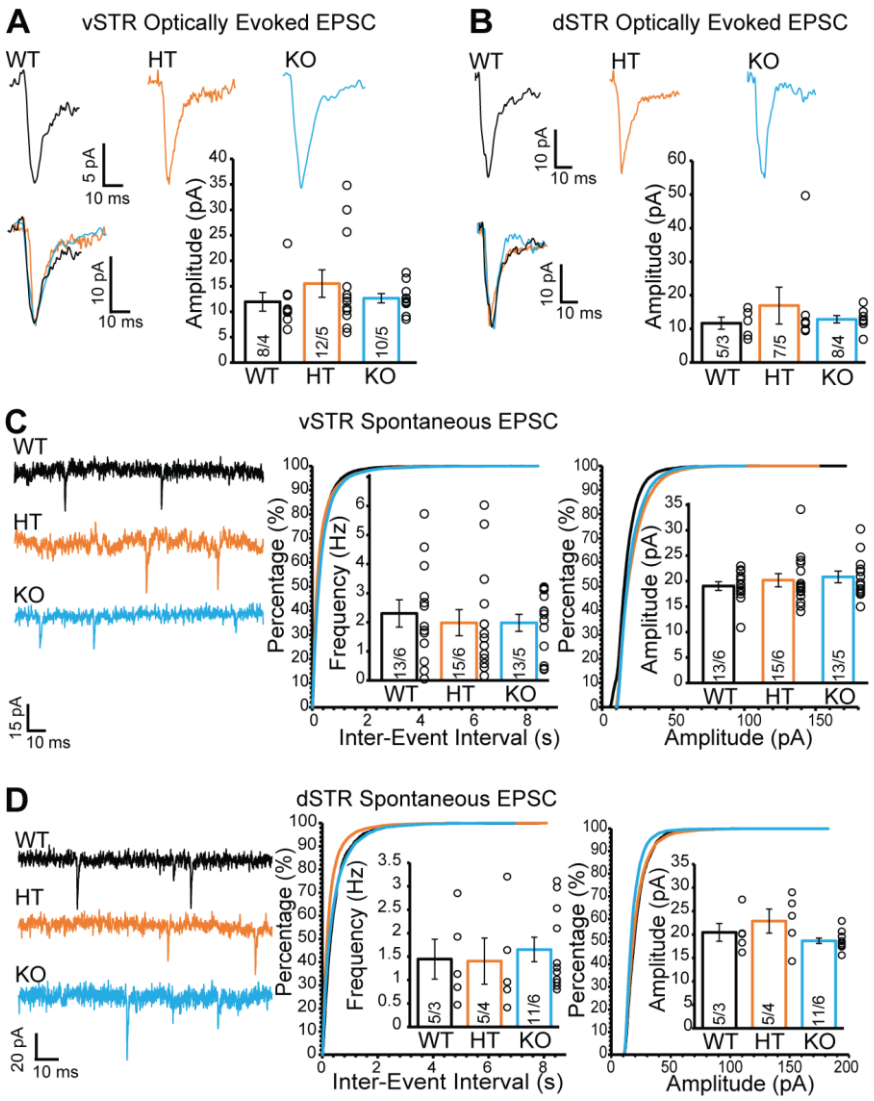

Figure 7 – Loss of neurexins does not influence glutamate release from dopamine neurons in the ventral and dorsal striatum. A- Representative traces (top) of EPSCs elicited by optical stimulation (o-EPSCs) and recorded in ventral striatal MSNs. Summary graph of o-EPSC amplitudes (bottom) shows no genotype effect. **B-** Representative traces (top) of o-EPSCs recorded in dorsal striatal MSNs. Summary graph of o-EPSC amplitudes (bottom) shows no genotype effect. **C**- Representative traces (left) of spontaneous EPSCs (sEPSC) recorded in ventral striatal MSNs. Cumulative distribution plots of sEPSC inter-event intervals (middle) and amplitudes (right); insets: summary graphs of average sEPSC frequency (middle) and amplitude (right). **D**- Representative traces (left) of spontaneous EPSC (sEPSC) recorded in dorsal striatal MSNs.

Cumulative distribution plots of sEPSC inter-event intervals (middle) and amplitudes (right); insets: summary graphs of average sEPSC frequency (middle) and amplitude (right). Data in summary graphs are provided as mean ± SEM. Statistical comparisons were performed with One-Way ANOVA (*P<0.05; **P<0.01; ***P<0.001; non-significant comparisons are not labeled). Tukey's correction was used for all multiple comparisons.

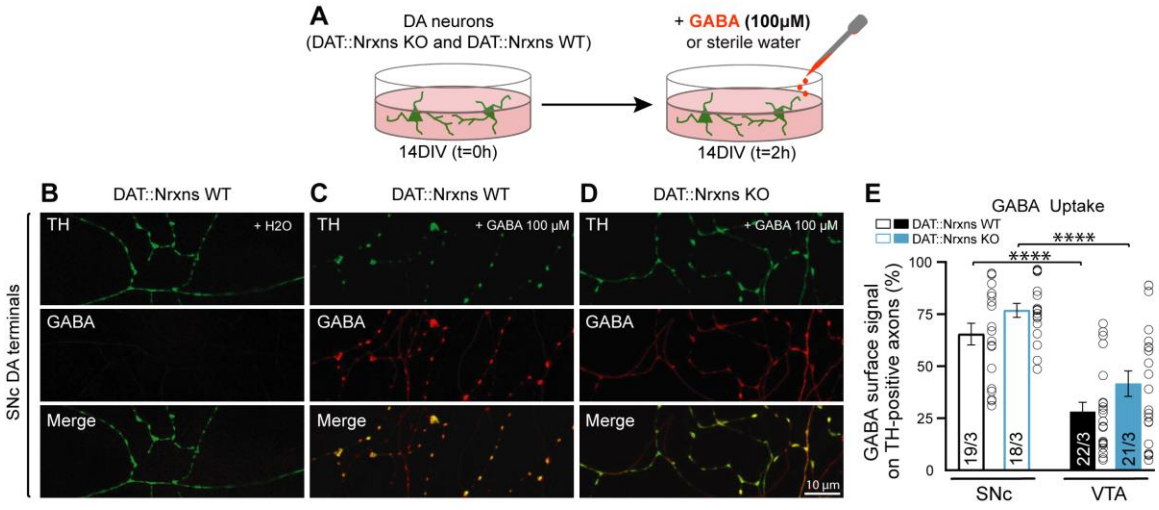

Figure 8 – **GABA uptake from cultured DA neurons is unchanged after conditional deletion of all neurexins. A –** Schematic representation of the experimental procedure for the GABA uptake assay in cultured DA neurons. **B** - **D**- Immunocytochemistry of SNc DA neurons from Nrxn123 WT (**B and C**) and DAT::NrxnsKO mice (**D**) for tyrosine hydroxylase (TH, green) and gamma-aminobutyric acid (GABA, red). **E** – Summary graph representing the quantification of GABA immunoreactivity signal surface in TH-positive axons for VTA and SNc DA neurons from DAT::NrxnsWT and KO cultures. N = 18-22 axonal fields from 3 different neuronal co-cultures. The number of observations represent the number of fields from TH-positive neurons examined. For all analyses, plots represent the mean ± SEM. Statistical analyses were carried out by 2-way

ANOVAs followed by Tukey's multiple comparison test. (*p < 0.05; **p < 0.01; ***p < 0.001; ****p < 0.0001).

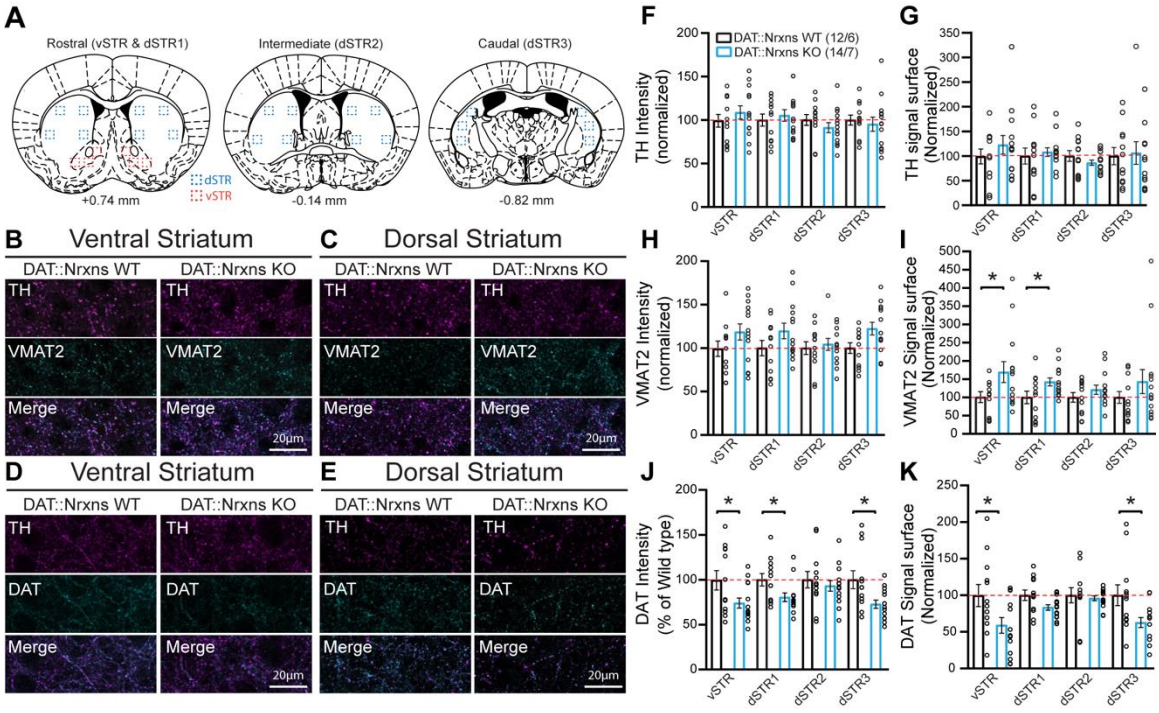

Figure 9 – Increased VMAT2 but decreased DAT expression in DA axon terminals lacking neurexins. A- Schematic representation of striatal slices used for immunohistochemistry characterization. Surface and intensity for each signal were measured in a series of 3 different striatal slices ranging from bregma +0.74 to bregma -0.82 mm, with a total of 14 different spots for each hemisphere. **B** and **C -** Immunohistochemistry of ventral (**B**) and dorsal (**C**) striatal slices from 8 week-old DAT::NrxnsKO and DAT::NrxnsWT mice (60X confocal) using tyrosine hydroxylase (TH, purple) and vesicular monoamine transporter 2 (VMAT2, blue) antibodies. **D** and **E -** Immunohistochemistry of ventral (**B**) and dorsal (**C**) striatal slices from DAT::NrxnsKO and DAT::NrxnsWT mice using TH (purple) and the dopamine transporter (DAT, blue) antibodies. **F** to **K -** Quantification of signal surface (% of WT) for TH, VMAT2 and DAT in the different striatal regions examined: "vSTR, dSTR1, dSTR2 and dSTR3" (DAT::NrxnsKO = 14 hemispheres/7 mice;

DAT::NrxnsWT = 12 hemispheres/6 mice). TH signal intensity: vSTR= 108.7 ± 7.48%; dSTR1= 105.2 ± 6.65%; dSTR2= 91.18 ± 5.71%; dSTR3= 95.26 ± 8.05% of control. TH surface area: vSTR= 122.6 ± 19.07%; dSTR1=107.9 ± 8.62%; dSTR2= 86.38 ± 5.42%; dSTR3= 106.20 ± 22.82% of control). VMAt2 intensity: vSTR= 118.4 ± 9.30%; dSTR1= 119.7 ± 8.96%; dSTR2= 104.3 ± 6.91%; dSTR3= 122.3 ± 7.24% of control. Statistical analysis was carried out by unpaired t-test for each substructure. Error bars represent ± S.E.M. (ns, non-significant; *, $p < 0.05$; **, $p < 0.01$; ***, $p < 0.001$; ****, $p < 0.0001$).

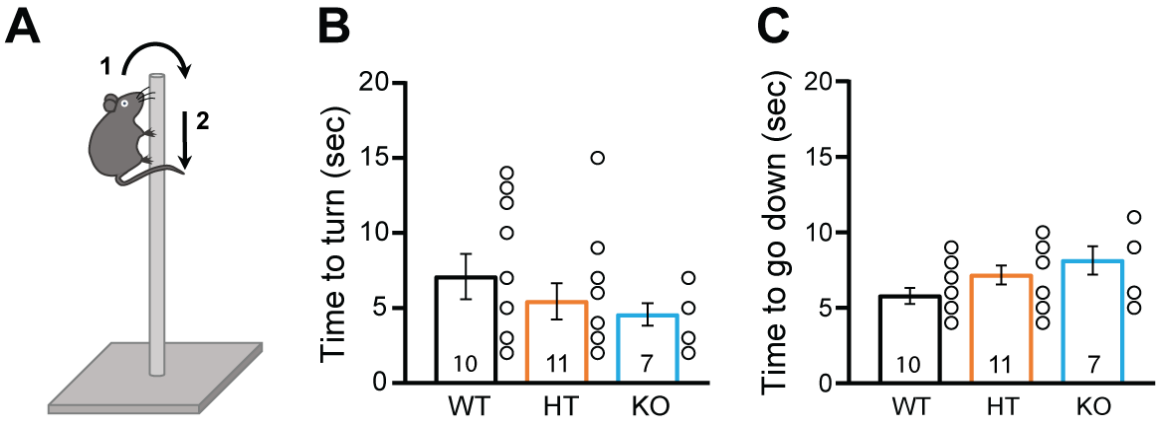

Supplemental Figure 1 - No motor deficit with the pole test in DAT::NrxnsKO mice. A- schematic representation of the pole test procedure. **B**- Summary graph of the time to turn shows no genotype effect (WT= 7.10 ± 1.50sec; HET= 5.45 ± 1.20sec; KO= 4.57 ± 0.75sec). **C**- Summary graph of the time to go down shows no genotype effect (WT= 5.80 ± 0.53sec; HET= 7.18 ± 0.62sec; KO= 8.14 ± 0.93sec).

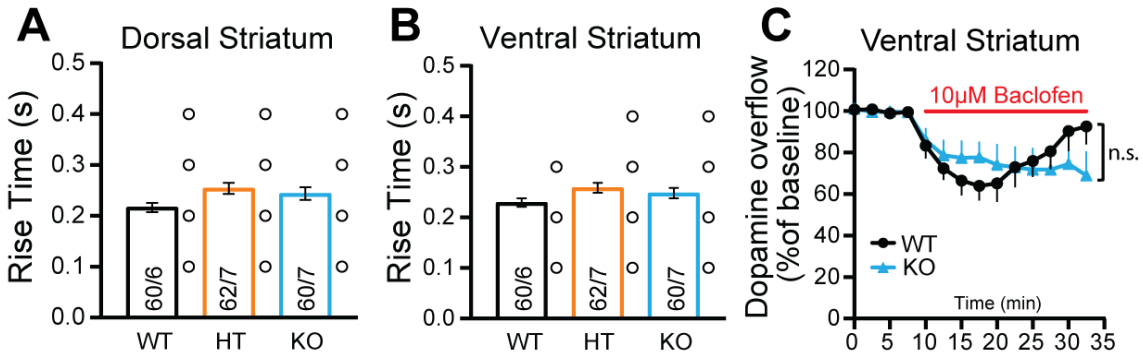

Supplemental Figure 2 – No change in $GABA_B$ receptor modulation of DA release after conditional deletion of all neurexins. A- Summary graph of the rise time of electrically evoked DA overflow in the dorsal striatum shows no genotype effect. **B-** Summary graph of the rise time of electrically evoked DA overflow in the ventral striatum shows no genotype effect. **C-** Plot of relative peak DA overflow and its modulation by the $GABA_B$ agonist baclofen in the ventral striatum. No difference between WT and KO mice was observed.

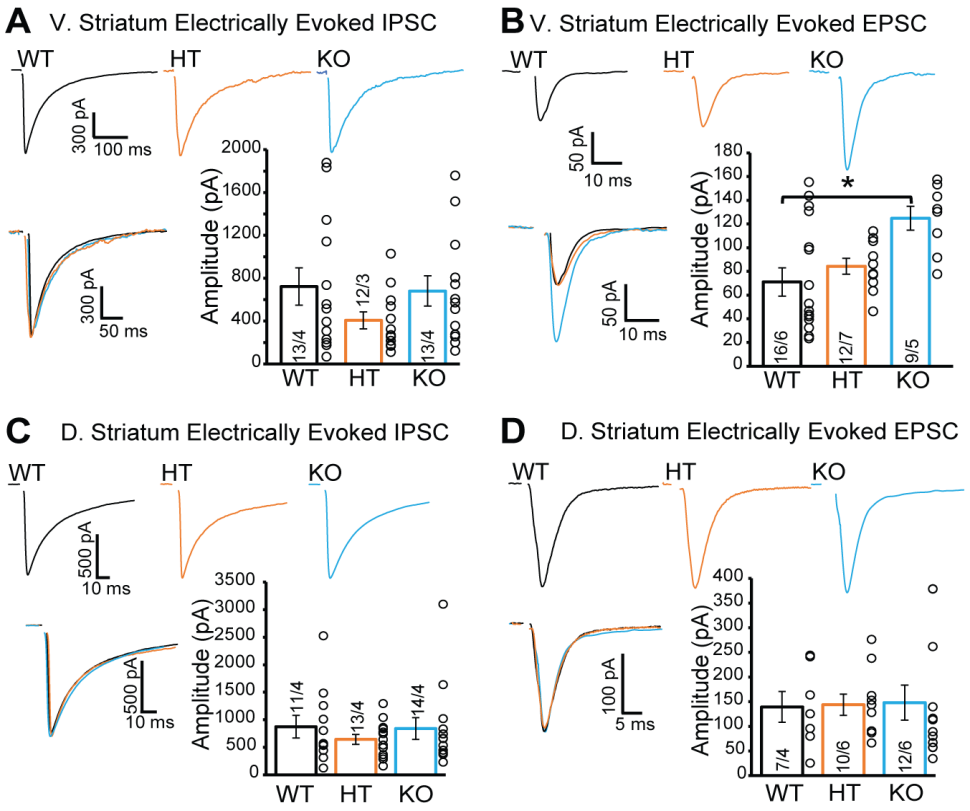

Supplemental Figure 3 – Electrically evoked EPSC amplitude is increased in the vSTR of DAT::NrxnsKO mice.

A- Representative traces (top) of IPSCs elicited by electrical-stimulation (e-IPSC) and recorded in ventral striatal MSNs. Summary graph of e-IPSC amplitudes (bottom) shows no genotype effect (*Peak Amplitude:* WT = -722.64 ± 174.29 pA, HT = -406.01 ± 80.15 pA, KO = -680.89 ± 141.06, Mean ± SEM). **B-** Representative traces (top) of EPSCs elicited by electrical-stimulation (e-EPSC) and recorded in ventral striatal MSNs. Summary graph of e-EPSC amplitudes (bottom) shows an increased amplitude in the KO mice compared to WT (Peak Amplitude: WT = -71.03 ± 11.9 pA, HT = -84.2 ± 6.76 pA, KO = -124.8 ± 10.15, Mean ± SEM). **C-** Representative traces (top) e-IPSCs recorded in dorsal striatal MSNs. Summary graph of e-IPSC amplitudes (bottom) shows no genotype effect. **D-** Representative traces (top) of e-EPSCs recorded in dorsal striatal MSNs. Summary graph of e-EPSC amplitudes (bottom) shows no genotype effect. Data in summary graphs

are presented as mean ± SEM; statistical comparisons were performed with One-Way ANOVA (*P<0.05; **P<0.01; ***P<0.001; non-significant comparisons are not identified). Tukey's correction was used for all multiple comparisons.

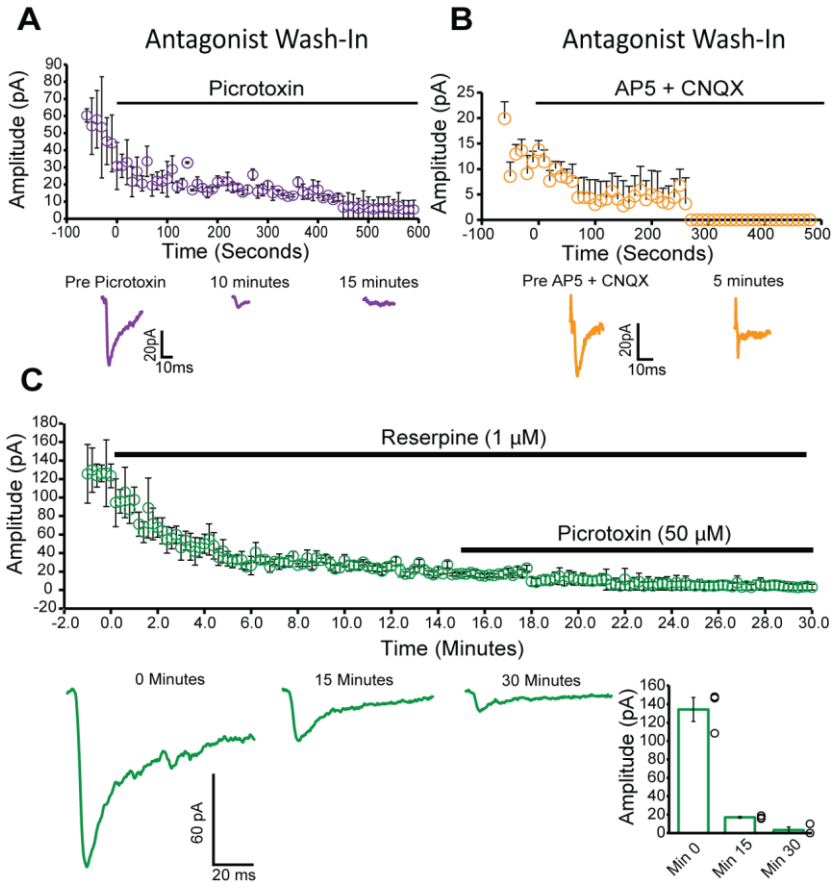

Supplemental Figure 4 – Pharmacological properties of o-IPSCs and o-EPSCs recorded from MSNs in acute ventral striatal slices. **A**- Graph showing the amplitude of o-IPSCs recorded in ventral striatal MSNs before and after incubation with the $GABA_A$ receptor blocker Picrotoxin. **B**-Graph showing the amplitude of o-EPSCs recorded in ventral striatal MSNs before and after incubation with the AMPA and NMDA receptor blockers AP5 and CNQX, respectively. **C**-Graph showing the amplitude of o-IPSCs recorded in ventral striatal MSNs before and after incubation with the VMAT2 blocker reserpine, followed by Picrotoxin.

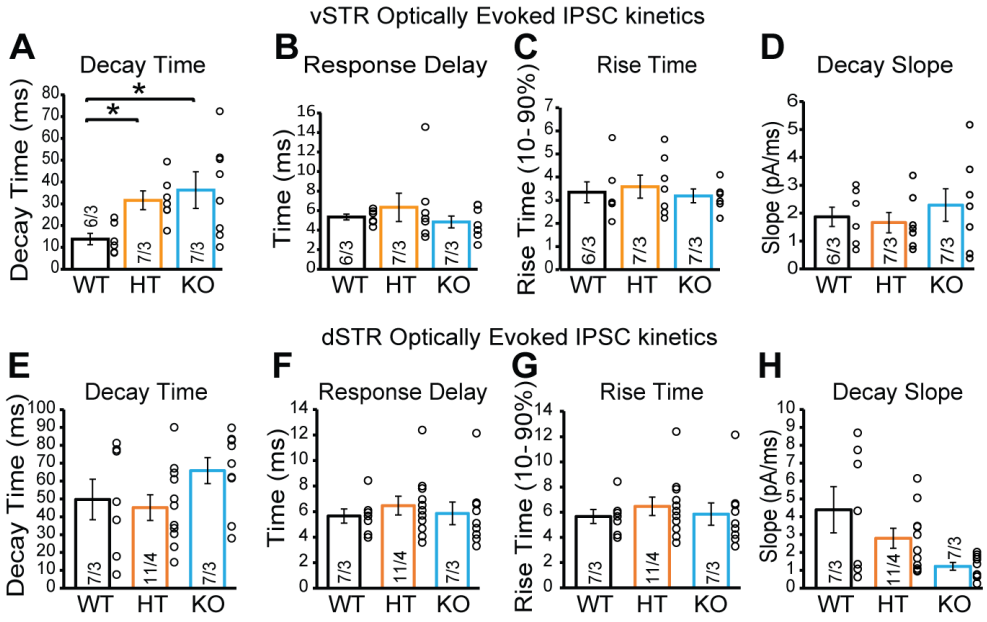

Supplemental Figure 5 –Removal of neurexins increases oIPSC decay time in the ventral but not the dorsal striatum. **A to D -** Summary graphs of o-IPSC kinetics recorded in ventral striatal MSNs. From left to right: decay time (**A**) (Tau: WT = 18.9 ± 2.8 ms, HT = 65.3 ± 13.5 ms, KO = 67.1 ± 21.8 ms, Mean ± SEM), response delay (latency from stimulation to peak response) (**B**), rise time (**C**), and decay slope (**D**). **E to H -** Summary graphs of o-IPSC kinetics recorded in dorsal striatal MSNs; (from left to right) decay time (**E**), response delay (**F**), rise time (**G**), and decay slope (**H**).

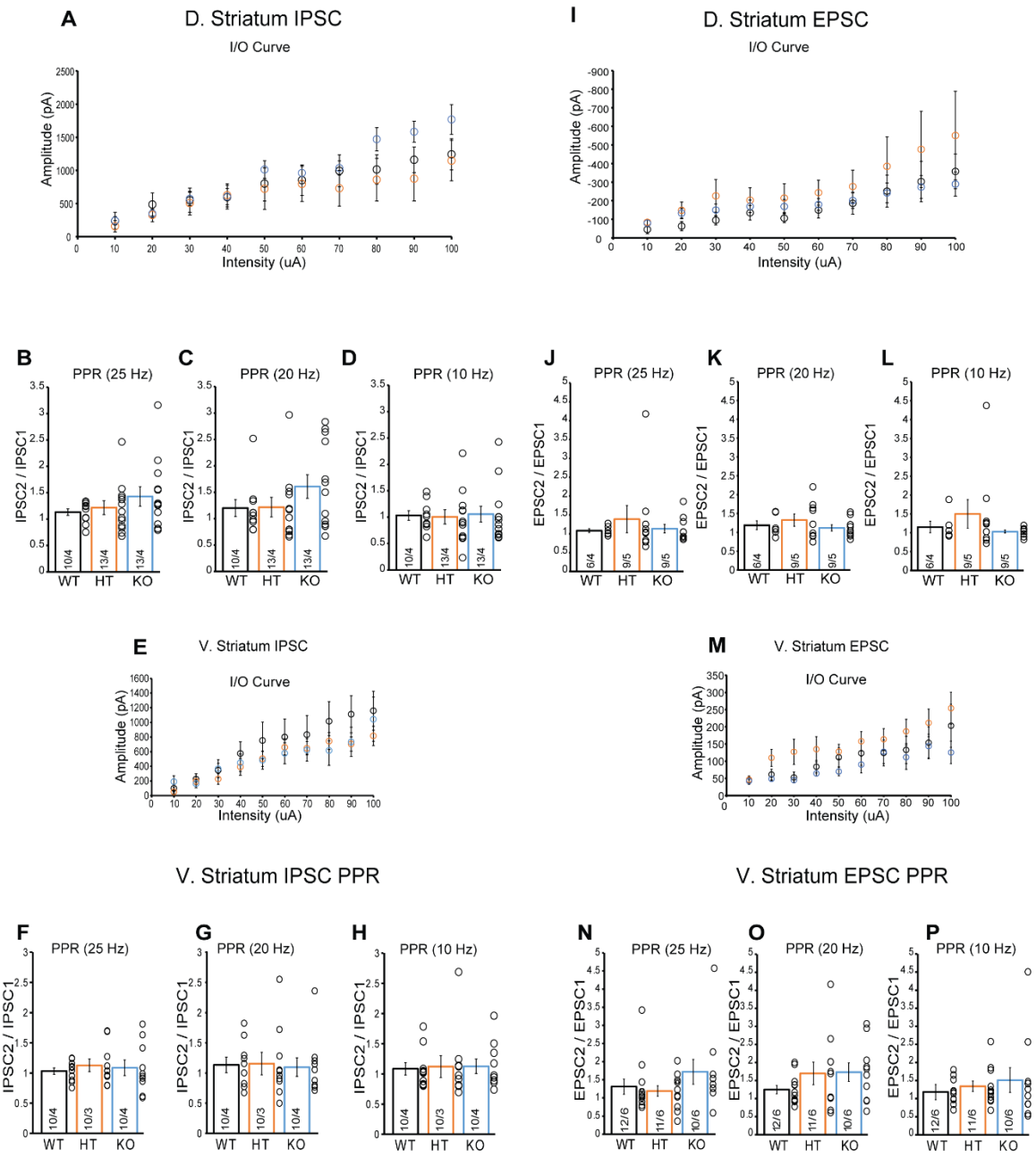

Supplemental Figure 6 – No change in synaptic plasticity of electrically-evoked IPSCs and EPSCs after conditional deletion of all Nrxns in DA neurons - A. Scatterplot of IPSC input-output relationship in MSNs of the dorsal striatum of WT, HT and KO mice. **B.** Summary graph of GABAergic IPSC paired-pulse ratio (PPR) in MSNs of the dorsal striatum; two electrical pulses were delivered with an inter-stimulation interval (ISI) of 40 ms (25 Hz). **C.** Same as in **B**; ISI = 50 ms (20 Hz). **D.** Same as in **B** and **C**; ISI = 100 ms (10 Hz). **E.** Scatterplot of IPSC input-output

relationship in MSNs of the ventral striatum. **F.** Summary graph of GABAergic IPSC paired-pulse ratio (PPR) in MSNs of the ventral striatum; two electrical pulses were delivered with an inter-stimulation interval (ISI) of 40 ms (25 Hz). **G.** Same as in **F**; ISI = 50 ms (20 Hz). **H.** Same as in **F** and **G**; ISI = 100 ms (10 Hz). **I.** Scatterplot of EPSC input-output relationship in MSNs of the dorsal striatum. **J.** Summary graph of glutamatergic paired-pulse ratio (PPR) in MSNs of the dorsal striatum; two electrical pulses were delivered with an inter-stimulation interval (ISI) of 40 ms (25 Hz). **K.** Same as in **J**; ISI = 50 ms (20 Hz). **L.** Same as in **K** and **J**; ISI = 100 ms (10 Hz). **M.** Scatterplot of EPSC input-output relationship in MSNs of the ventral striatum. **N.** Summary graph of EPSC paired-pulse ratio (PPR) in MSNs of the ventral striatum; two electrical pulses were delivered with an inter-stimulation interval (ISI) of 40 ms (25 Hz). **O.** Same as in **N**; ISI = 50 ms (20 Hz). **P.** Same as in **N** and **O**; ISI = 100 ms (10 Hz).

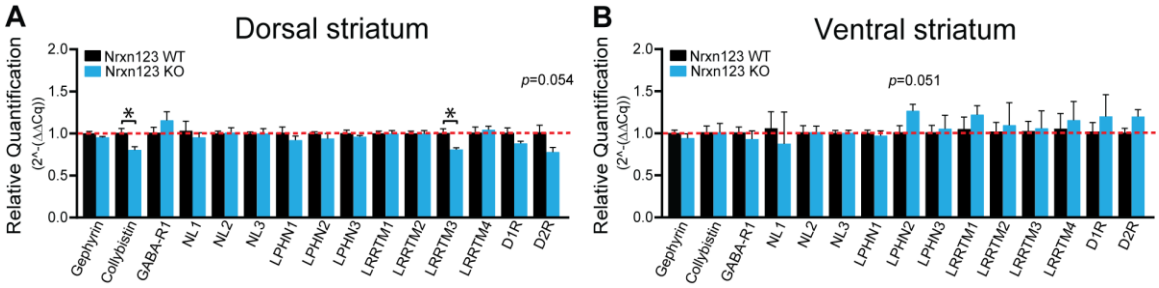

Supplemental Figure 7 - Gene expression profile in target cells of DA neurons after conditional deletion of Nrxn123. A and **B**– Relative changes of mRNA levels measured by RT-qPCR, from ventral and dorsal striatum tissue: Gephyrin (Gphn), Collybistin (Arhgef 9), GABA-A receptor (Gabra1), Neuroligins 1, 2 and 3 (Nlgn1, 2 and3), Latrophilins 1, 2 and 3 (Lphn1, 2 and 3), LRRTMs 1, 2, 3, 4 (LRRTM1, 2, 3 and 4), D1R (DRD1) and D2R (DRD2) in brain tissue from P80 DAT::NrxnsWT, and DAT::NrxnsKO mice.

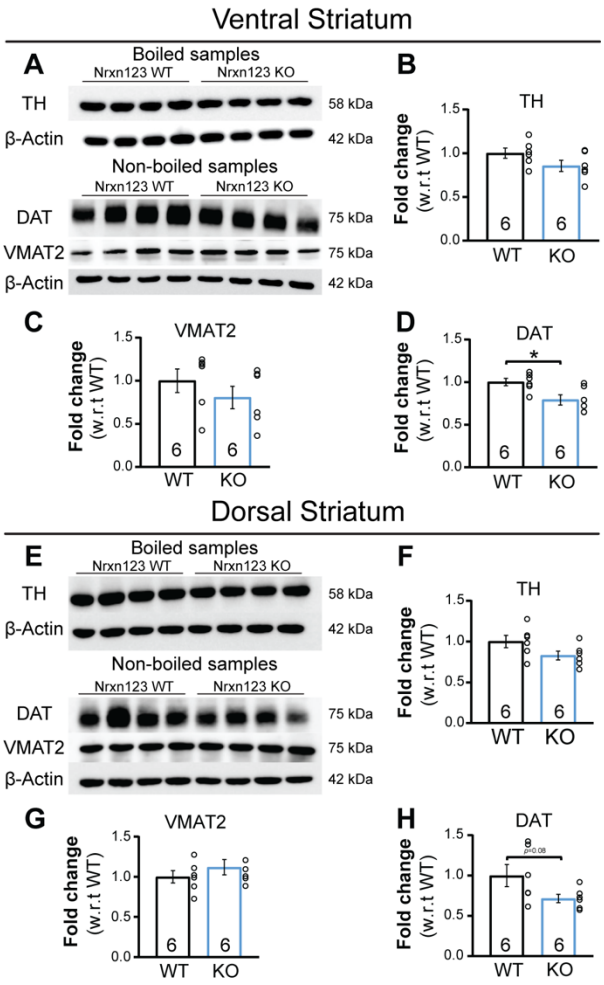

Supplemental Figure 8 – Decrease of DAT protein expression in DA neurons from DAT::NrxnsKO mice. A- Representative western blots illustrating TH, DAT, VMAT2 and β-actin protein from total striatum homogenates of adult mice. **B to D-** Immunoblot quantifying relative protein levels (fold change compared to controls) for TH (**B**), VMAT2 (**C**) and DAT (**D**) (n = 6 DAT::NrxnsWT, HET and KO mice). **E-** Representative western blots illustrating TH, DAT, VMAT2 or β-actin from total striatum homogenates of adult mice. **F to H-** Immunoblot quantifying relative protein levels (fold change compared to controls) for TH (**F**), VMAT2 (**G**) and DAT (**H**) (n = 6 DAT::NrxnsWT, HET and KO mice). Error bars represent ± S.E.M. (ns, non-significant; *, $p < 0.05$; **, $p < 0.01$; ***, $p < 0.001$; ****, $p < 0.0001$).

Supplementary table 1 – qPCR primers for ventral and dorsal striatum

Gene	Oligo Forward	Oligo Reverse	Reference Sequences
Gphn	cctcgcccagaataccac	gacggctgctcatctgattac	NM_145965.2, NM_172952.3
Arhgef9	tgagaaaagcttctaaacagaaagg	gtactggccctggtttaacg	NM_001033329.3
Gabra1	cgatcctctctcccacactt	tttcttcatcacgggcttg	NM_010250.5
Nlgn1	ctatcggcttggggtacttg	caaggagcccgtagtttcct	NM_138666.3, NM_001163387.1
Nlgn2	gaggaaaggggaatctctg	ggccgtgggaaggtaagt	NM_198862.2
Nlgn3	gaagggagggctccaagat	ggtccttctccttggtctgat	NM_172932.4
Adgrl1	cagtacgactgtgtcccttacatc	cagactgatgctctgactcatgt	NM_181039.2
Adgrl2	gagctgaagccgagtgagaa	cctgcatgtcttctctcgttt	NM_001081298.1
Adgrl3	aacaacctccttcagccaca	cgcagttgatcacttgtcgt	NM_001347369.1
Lrrtm1	cgccctgcatataattagcc	gaagcgctgggtcagaaa	NM_028880.3
Lrrtm2	gtagggacaaaaacctgtttgatt	aagtaggaagccagttgtggtc	NM_178005.4
Lrrtm3	gaccctgcacctatagcaaatc	tgccagaaaggttgacacat	NM_178678.4
Lrrtm4	gccatgattctcctggtgat	tgagtgctgttggagttgtttc	NM_001134743.1
Drd1	aggttgagcaggacatacgc	tggctacggggatgtaaaag	NM_010076.3
Drd2	gatgcttgccattgttcttg	attcaggatgtgcgtgatga	NM_010077.2
Gapdh	tgtccgtcgtggatctgac	cctgcttcaccaccttcttg	NM_008084.2
Actb	aaggccaaccgtgaaaagat	gtggtacgaccagaggcatac	NM_007393.3

Supplementary table 2 – Antibodies for Western Blot

Antibody	Catalog numbers	Raised in	Dilution used	RRID
DAT	MAB369 (Millipore)	Rat	1:1000	AB_2190413
TH	MAB318 (Millipore)	Mouse	1:1000	AB_2201528
VMAT2	Kind gift from Dr. Gary Miller, Emory University, USA	Rabbit	1:5000	NA
β-Actin	A3854(Sigma)	Purified from hybridoma cell culture	1:15000	AB_262011

Antibody	Catalog number	Dilution used	RRID
Peroxidase-conjugated AffiniPure Goat Anti-Rat IgG (H+L)	711-035-152 (Cedarlane)	1:5000	AB_10015282
Peroxidase-conjugated AffiniPure Goat Anti-Rabbit IgG (H+L)	112-035-003 (Cedarlane)	1:5000	AB_2338128
Peroxidase-conjugated AffiniPure Goat Anti-Mouse IgG (H+L)	115-035-146 (Cedarlane)	1:5000	AB_2307392